UC San Diego
UC San Diego Previously Published Works

Title
Automated longitudinal intra-subject analysis (ALISA) for diffusion MRI tractography

Permalink
https://escholarship.org/uc/item/1gb937h2

Authors
Aarnink, Saskia H
Vos, Sjoerd B
Leemans, Alexander
et al.

Publication Date
2014-02-01

DOI
10.1016/j.neuroimage.2013.10.026

Peer reviewed
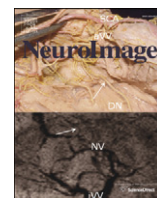
Automated longitudinal intra-subject analysis (ALISA) for diffusion MRI tractography

Saskia H. Aarnink [a,b,1], Sjoerd B. Vos [a,*,1], Alexander Leemans [a], Terry L. Jernigan [c,d,e,f], Kathrine Skak Madsen [c,d], William F.C. Baaré [c]

[a] Image Sciences Institute, University Medical Center Utrecht, the Netherlands
[b] Elkerliek Hospital, Medical Physics, Helmond, The Netherlands
[c] Danish Research Centre for Magnetic Resonance, Centre for Functional and Diagnostic Imaging and Research, Copenhagen University Hospital Hvidovre, Denmark
[d] Center for Integrated Molecular Brain Imaging, Copenhagen, Denmark
[e] Faculty of Health Sciences, University of Copenhagen, Copenhagen, Denmark
[f] Center for Human Development, University of California, San Diego, La Jolla, CA, USA

ARTICLE INFO

ABSTRACT

Fiber tractography (FT), which aims to reconstruct the three-dimensional trajectories of white matter (WM) fibers non-invasively, is one of the most popular approaches for analyzing diffusion tensor imaging (DTI) data given its high inter- and intra-rater reliability and scan-rescan reproducibility. The major disadvantage of manual FT segmentations, unfortunately, is that placing regions-of-interest for tract selection can be very labor-intensive and time-consuming. Although there are several methods that can identify specific WM fiber bundles in an automated way, manual FT segmentations *across multiple subjects* performed by a trained rater with neuroanatomical expertise are generally assumed to be more accurate. However, for longitudinal DTI analyses it may still be beneficial to automate the FT segmentation *across multiple time points*, but then for each individual subject separately. Both the inter-subject and intra-subject automation in this situation are intended for subjects without gross pathology. In this work, we propose such an automated longitudinal intra-subject analysis (dubbed ALISA) approach, and assessed whether ALISA could preserve the same level of reliability as obtained with manual FT segmentations. In addition, we compared ALISA with an automated *inter-subject* analysis. Based on DTI data sets from (i) ten healthy subjects that were scanned five times (six-month intervals, aged 7.6–8.6 years at the first scan) and (ii) one control subject that was scanned ten times (weekly intervals, 12.2 years at the first scan), we demonstrate that the increased efficiency provided by ALISA does not compromise the high degrees of precision and accuracy that can be achieved with manual FT segmentations. Further automation for *inter-subject* analyses, however, did not provide similarly accurate FT segmentations.

© 2013 Elsevier Inc. All rights reserved.

Introduction

To date, diffusion magnetic resonance imaging (MRI) is the only non-invasive method for probing soft tissue microstructure and its 3D architectural organization in vivo, offering the possibility of exploring the microstructural organization and architectural configuration of distinct anatomical fiber networks within the brain white matter (WM) (Jones, 2008; Tournier et al., 2011). Diffusion tensor imaging (DTI) (Basser et al., 1994), in particular, has been widely used to investigate e.g., WM abnormalities in pathological conditions

(Caeyenberghs et al., 2010; Ciccarelli et al., 2006; Concha et al., 2005a, b, 2009; Deprez et al., 2011; Jones et al., 2006; Price et al., 2008; Sage et al., 2009; Van Hecke et al., 2010b; Yogarajah et al., 2008), WM changes in normal development (Eluvathingal et al., 2007; Lebel et al., 2008, 2010; Verhoeven et al., 2010; Zhang et al., 2007), and aging (Hsu et al., 2008, 2010; Sullivan and Pfefferbaum, 2007; Van Hecke et al., 2008a). In many of these studies, fiber tractography (FT) (Basser et al., 2000; Conturo et al., 1999; Jones et al., 1999a; Koch et al., 2001; Mori et al., 1999; Parker et al., 2002, 2003; Poupon et al., 2000) has been used to identify specific WM fiber bundles, from which diffusion characteristics, such as fractional anisotropy (FA) and mean diffusivity (MD), can be derived (Jones et al., 2005a). Other approaches for investigating DTI data include region-of-interest (ROI) (e.g., Madsen et al., 2011; Snook et al., 2005), histogram (e.g., Cercignani et al., 2001), voxel-based (e.g., Giorgio et al., 2010) including TBSS (Smith et al., 2006), network-based (e.g., Hagmann et al., 2008; Reijmer et al., 2013) and atlas-based (e.g., Faria et al., 2011) analyses. A detailed

* Corresponding author at: Image Sciences Institute, University Medical Center Utrecht, Heidelberglaan 100, Location AZU, Room Q.S.4.300, Utrecht, 3584 CX, The Netherlands. Fax: +31 30 251 3399.
E-mail address: Sjoerd@isi.uu.nl (S.B. Vos).
URL: http://www.isi.uu.nl/People/?sjoerd (S.B. Vos).
[1] These authors contributed equally.

description of these techniques is considered beyond the scope of this article — the interested reader is referred to surveys by Cercignani (2010) and Hasan et al. (2011).

With the ability to observe diffusion changes over time in the same population of subjects, longitudinally designed DTI studies can provide more specific insights into the microstructural dynamics of brain WM tissue compared to studies with a cross-sectional population setup (Beaulieu, 2002; Johansen-Berg, 2010; Lebel and Beaulieu, 2011). Boosted by the advent of more stable and high performance MR equipment, the interest to perform longitudinal DTI studies for capturing such subject-specific changes in microstructural organization is increasing rapidly (e.g., Concha et al., 2007; Deprez et al., 2012; Gong et al., 2008; Keller and Just, 2009; Kumar et al., 2009; Ljungqvist et al., 2011; Schlaug et al., 2009; Scholz et al., 2009; Sullivan et al., 2010; Yogarajah et al., 2010). Although there are several well-established methods for analyzing *cross-sectional* DTI data sets, they may not be 'optimal' for *longitudinal* studies. In voxel-based DTI analyses, for instance, which are notorious for their high sensitivity with respect to the amount/type of filtering (Jones et al., 2005b; Van Hecke et al., 2009, 2010a) and choice of template/atlas (Sage et al., 2009; Van Hecke et al., 2008b, 2011), subtle intra-subject changes may not be detected due to the much larger residual inter-subject misalignments. In this case, and if there is also a clear hypothesis regarding a specific WM fiber bundle (or a segment thereof — Colby et al., 2012), FT may be preferred over the voxel-based approach.

By combining *objective* protocols for extracting WM fiber pathways of interest on the one hand (Catani and Thiebaut de Schotten, 2008; Wakana et al., 2004, 2007) and incorporating *subjective* prior knowledge from the neuroanatomical expert on the other hand, many studies have already demonstrated the high inter- and intra-rater reliability and scan–rescan reproducibility of manual FT segmentations (Ciccarelli et al., 2003; Danielian et al., 2010; Heiervang et al., 2006; Kristo et al., 2013,in press; Malykhin et al., 2008; Pfefferbaum et al., 2003; Wakana et al., 2007). The major drawback of manual FT segmentations, however, is that placing ROIs for tract selection can be very labor-intensive and time-consuming, which – for obvious reasons – can become problematic for large-cohort studies. Notwithstanding the existence of methods that can identify WM fiber bundles in an automated way in the absence of gross pathology (Clayden et al., 2007; Hagler et al., 2009; Lebel et al., 2008; Leemans et al., 2006; O'Donnell et al., 2009; Reich et al., 2010; Suarez et al., 2012; Verhoeven et al., 2010; Yendiki et al., 2011; Zhang et al., 2010), manual FT segmentations *across multiple subjects* performed by a trained rater with neuroanatomical expertise are generally more specific and, therefore, more accurate. For longitudinal DTI analyses, however, it may still be beneficial to automate the FT segmentation *across multiple time points*, but then for each individual subject separately. In doing so, the adverse effect of inter-subject variability on the reliability of the FT results may be circumvented, while maintaining the main advantages of the automated approach, i.e., higher efficiency and objectivity.

In this work, we developed an automated longitudinal intra-subject analysis (ALISA) for investigating FT segmentations and compared its performance in terms of precision and accuracy to the "bronze standard", i.e. the manual FT segmentations. In addition, we compared these results to those obtained with FT segmentations obtained in an automated way over all time points *and* all subjects (Lebel et al., 2008). Sixty DTI data sets, which are part of the HUBU cohort database ("Hjernens Udvikling hos Børn og Unge": Brain maturation in children and adolescents; see Madsen et al., 2010, 2011 for more details), were included in this study: five acquisitions at six-month intervals for ten healthy subjects and a set of ten repeats of one control subject scanned at weekly intervals. Important to note here is that these automated methods are not intended for case-based clinical use in cases with gross pathology, but rather for the use of longitudinal group studies of healthy development and aging, and pathologies without large displacing lesions.

Without loss of generality, the analyses were evaluated with tractography results from four WM fiber bundles: (i) the superior segment of the cingulum (SSCing) bundle, part of the collection of WM fibers that interconnect limbic structures, relevant for the regulation of emotional processes (e.g., Karaus et al., 2009); (ii) the cortico-spinal tracts (CST), running from the spinal cord to the motor cortex; (iii) the uncinate fasciculus (UF), connecting the frontal and temporal lobes, which has been shown to be important in the interaction between cognition and emotion (e.g., Price et al., 2008); and (iv) the forceps major (FM), or splenium of the corpus callosum, providing interhemispheric occipital connections that are affected in, for instance, schizophrenia (Catani and Thiebaut de Schotten, 2008; Clark et al., 2011).

Material and methods

Subjects and data acquisition

Sixty DTI data sets were acquired for this study, five acquisitions at six-month intervals for ten healthy subjects (8 F/2 M) aged 7.6 to 8.6 years (mean age of 8.1 ± 0.4 years) at the first acquisition date and a set of ten repeats of one control subject (female, age 12.2 years) scanned on four occasions, with respectively two, three, two, and three separate scan sessions. These four occasions were separated by two, two, and seven weeks, respectively. The data sets are part of the HUBU cohort database (see Madsen et al., 2010, 2011 for more details) and have been acquired on a 3 T Siemens Magnetom Trio MR scanner (Siemens, Erlangen, Germany) with an 8-channel head coil (Invivo, FL, USA) using a twice-refocused balanced spin echo sequence that minimized eddy current distortions (Reese et al., 2003) (TR/TE = 8200/100 ms) with a b-value of 1200 s/mm^2 along 61 directions using the electrostatic repulsion method (Jansons and Alexander, 2003; Jones et al., 1999b) available in CAMINO (Cook et al., 2006), ten b = 0 s/mm^2 images, and with a GRAPPA factor of 2. The acquisition matrix of 96×96 comprised a field-of-view of 220×220 mm^2 (2.3 mm in-plane resolution) and 61 axial slices were acquired with thickness 2.3 mm and without gap (Jones and Leemans, 2011).

DTI pre-processing

The diffusion-weighted (DW) images were corrected for head motion and eddy current induced geometric distortions using a global affine registration procedure, as described in Leemans and Jones (2009). In this correction procedure, the DW data were transformed directly to the ICBM-DTI-81 template ($2 \times 2 \times 2$ mm^3) in MNI space (Mori et al., 2008; Rohde et al., 2004) by applying cubic interpolation with only a single resampling step (i.e., concatenation of transformation matrices), thereby keeping artificial data smoothing to a minimum (Klein et al., 2010). We explicitly used a 'rigid' transformation model (only 3D rotations and translations) to ensure that no additional confounds, such as partial volume effect (PVE) related modulations of the estimated DTI measures (Vos et al., 2011), were introduced in this processing step. Note that for the analyses applied in this study, inter-subject alignment was not required. However, by transforming all data sets to a common reference space, uniformity in terms of brain angulation was maximized across subjects, which facilitated the definition of standardized protocols for extracting the WM fiber bundles of interest (as for instance also done in Caeyenberghs et al., 2010). Finally, the diffusion tensor was estimated with the RESTORE approach (Chang et al., 2005) and the FA, MD, and radial/axial (RD/AD) diffusivities were subsequently computed (Pierpaoli and Basser, 1996).

Fiber tractography

For each DTI data set, whole-brain deterministic fiber tracking (as described by Basser et al., 2000) was performed using *ExploreDTI*
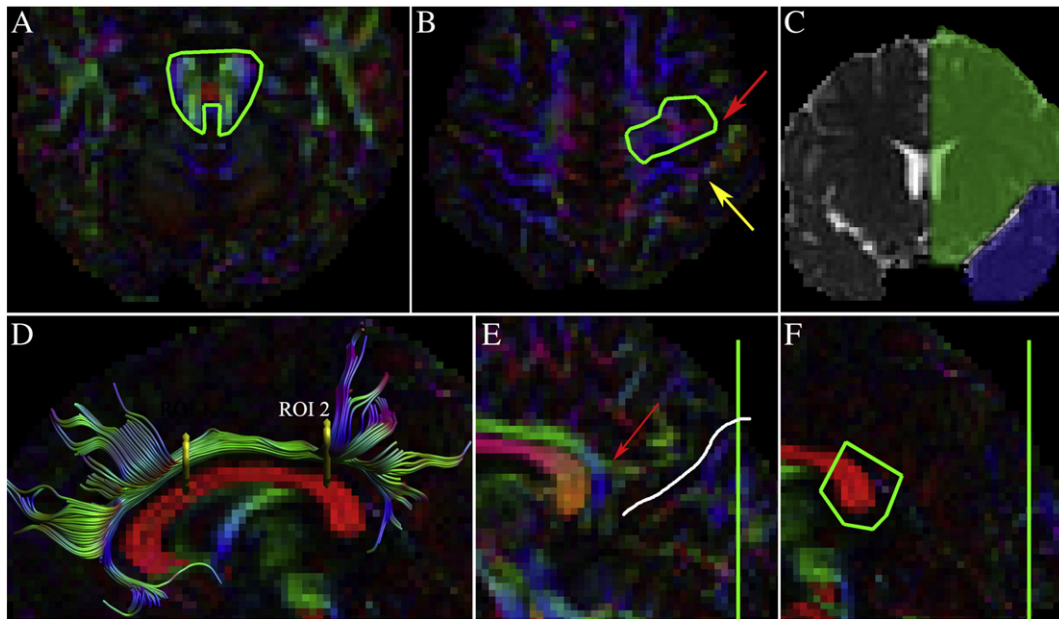
Fig. 1. Delineation of ROIs for the segmentation of fiber tracts. For the cortico-spinal tracts, two 'AND' ROIs were defined: one on the axial slice showing the decussation of the superior cerebellar peduncles (the "red dot", in A); and one on the most inferior axial slice where M1 (green ROI) and S1 (yellow arrow) are clearly separated by the central sulcus (indicated by the red arrow). 'NOT' gates were placed at the midsagittal slice and anterior to the cerebellum (B). For the segmentation of the uncinate fasciculus (C), two 'AND' ROIs were placed on the most posterior coronal slice where the Sylvian fissure (indicated in yellow in A) still clearly separates the frontal lobe (green ROI) from the temporal lobe (blue ROI). For the delineation of the superior segment of the cingulum bundle two 'AND' ROIs were defined (D): one on the most posterior coronal slice in which the genu of the corpus callosum could be seen in full profile; the second 'AND' ROI was defined by the most anterior coronal slice in which the splenium of the corpus callosum could be seen in full profile. For the forceps major, one on the sagittal slice that most clearly shows the perisplenial cingulum (red arrow in E), the parieto-occipital sulcus is detected (white line in E) and 'AND' ROIs are drawn on a coronal slice around the occipital lobes at the posterior edge of this sulcus (green line). On the midsagittal slice another ROI is drawn around the splenium of the corpus callosum (F).

(Leemans et al., 2009) with the following parameters: an isotropic 2 mm seed point resolution was applied throughout the entire brain; the FA thresholds for seed point selection and termination of tracking were 0.2; the angle threshold was 30°; and the step size was set to 1.0 mm. Tract selection ROIs ('AND' gates) were defined according to specific protocols (Catani and Thiebaut de Schotten, 2008; Conturo et al., 1999; Hasan et al., 2009; Wakana et al., 2004, 2007) to extract the SSCing, CST, and UF bilaterally and the FM from the whole-brain tractography results. 'NOT' ROIs, which exclude tract pathways not-of-interest, were placed only on predefined locations, identical for each data set, to minimize 'subjective tract-editing'. The FT segmentations were all performed by a trained medical physicist (S.H.A.) for the UF an SSCing and a neurobiologist (K.S.M.) for the FM and the CST. All raters were blinded to subject identification, time of scan, and brain hemisphere. Intra- and inter-rater reliability of this approach has been demonstrated in previous studies and is therefore considered beyond
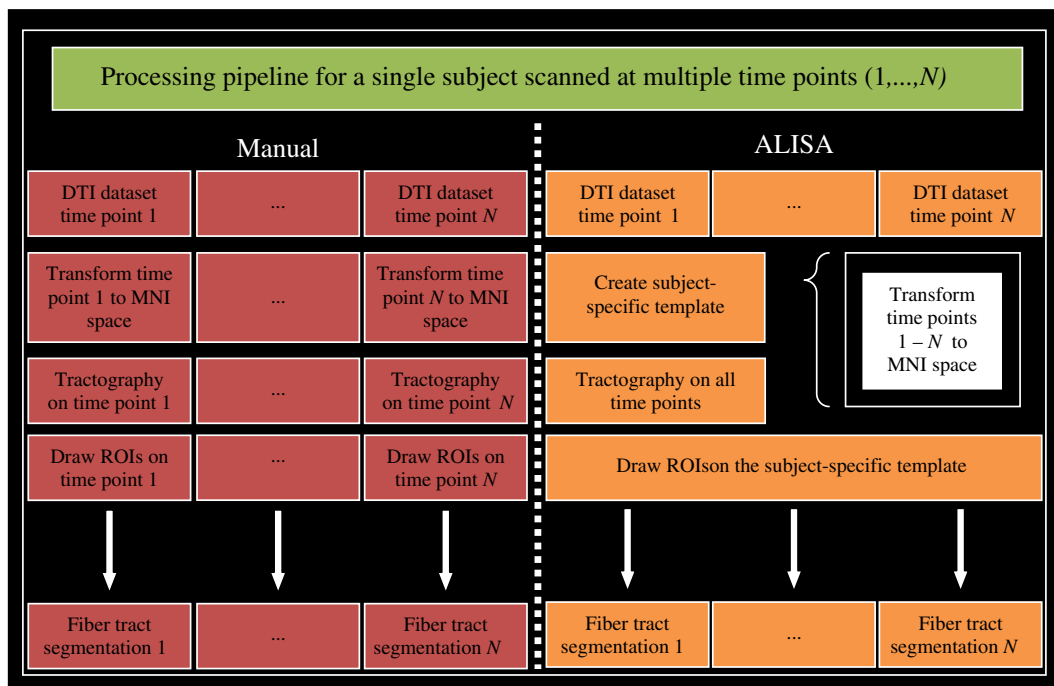
Fig. 2. Flow chart providing a schematic overview of the proposed automated longitudinal intra-subject analysis (ALISA) and manual fiber bundle segmentation approaches.

the scope of this work (e.g., Ciccarelli et al., 2003; Danielian et al., 2010; Malykhin et al., 2008; Pfefferbaum et al., 2003). For each reconstructed fiber bundle, average FA, MD, AD, RD, and tract volume were computed. The following sections provide a detailed description of the protocols that were applied to extract the four fiber bundles.

Cortico-spinal tracts

To isolate the CST (see Figs. 1A, B), two axial 'AND' gates were placed selecting the pons and the motor cortex (M1) as described in Wakana et al. (2007). The first 'AND' gate was drawn on the slice of the pons where the decussation of the cerebellar peduncles is most visible (i.e., the 'red spot', Fig. 1A); the latter was drawn on the most inferior axial slice where the central sulcus clearly separates S1 and M1 (Fig. 1B). On the mid-sagittal slice, a 'NOT' gate was placed to exclude false-positive pathways, such as spurious interhemispheric tracts. Another 'NOT' ROI was placed between the pons and the cerebellum to exclude the cerebellar tracts.

Uncinate fasciculus

To select the UF, two 'AND' gates were placed on the most posterior coronal slice where the Sylvian fissure still clearly separates the frontal lobe from the temporal lobe as in Wakana et al. (2007) and Hasan et al. (2009). This slice was selected on the MD map, where the cerebrospinal fluid (CSF) provides a clear demarcation for separating these two brain regions. As shown in Fig. 1C, one ROI (blue) was placed around the temporal lobe, and another ROI (green) was placed around the frontal lobe. A 'NOT' ROI was placed on the midsagittal slice to exclude false-positive pathways, such as spurious interhemispheric tracts.

Superior segment of the cingulum

A consistent reconstruction of the *entire* cingulum bundle with DTI-based FT is known to be extremely difficult as the regions in which this tract terminates can differ substantially across multiple subjects due to error accumulation during tract propagation. To minimize the contribution of non-specific pathways only the *superior segment* of the
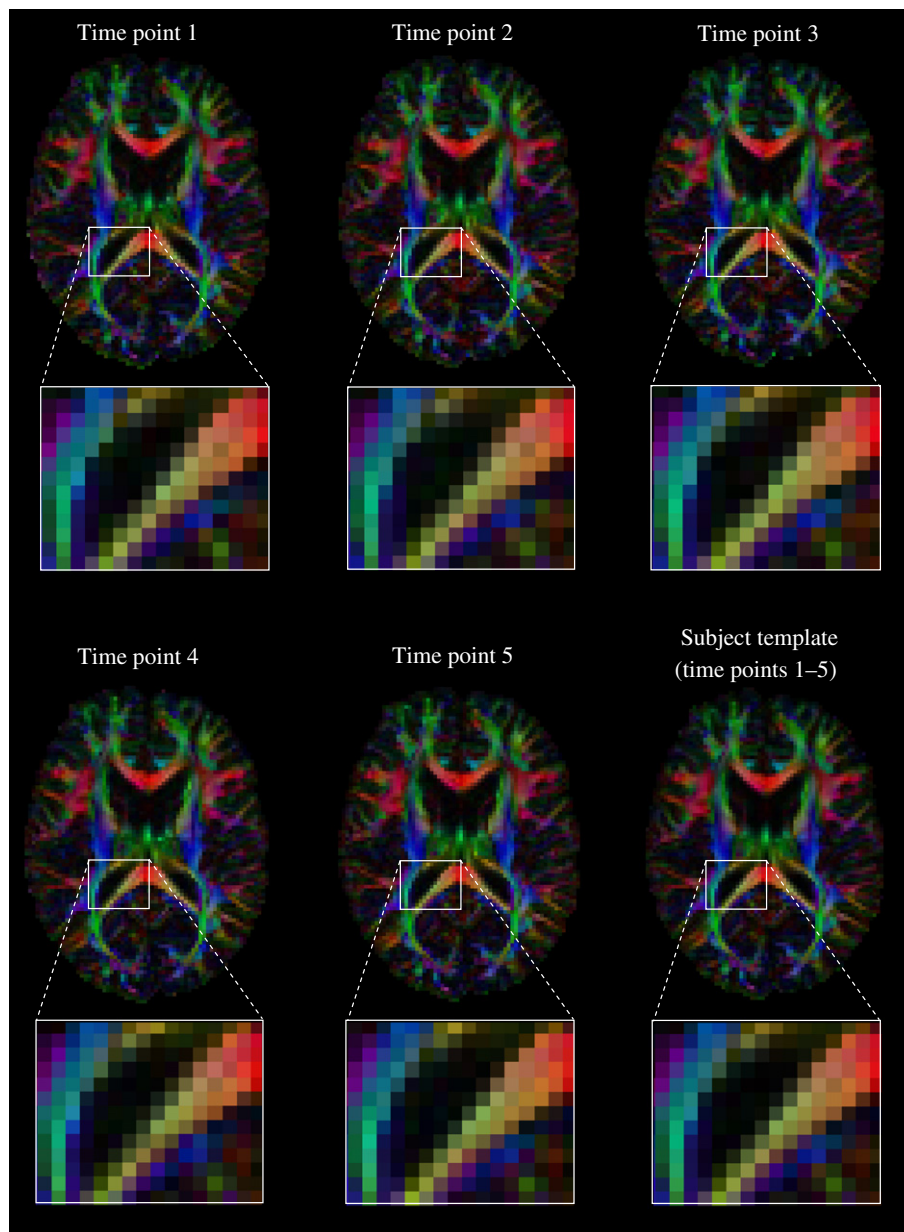
Fig. 3. Directionally color-encoded fractional anisotropy maps of a representative subject: each slice represents a different time point (5 scans with 1/2 year intervals); the right bottom image represents the subject-specific template (derived from the five data sets). These axial slices indicate the same location in the brain; the enlarged regions demonstrate the high level of spatial alignment across the different time points.

cingulum (SSCing) was selected (Emsell et al., 2009). The SSCing was defined by two 'AND' gates: one on the most posterior coronal slice, that would still show the genu of the corpus callosum, and one on the most anterior coronal slice in which the splenium of the corpus callosum was seen in full profile (see Fig. 1D).

Forceps major

The FM was segmented by placing two 'AND' gates around the occipital lobe, i.e., one around each hemisphere to specifically capture the interhemispheric occipital connections. More specifically, for each hemisphere the sagittal slice showing the perisplenial part of the cingulum was found, and the parieto-occipital sulcus was defined on this slice (Fig. 1E). The 'AND' gate was then drawn on the most posterior edge of the sulcus on the corresponding coronal slice, around only the occipital lobe (Wakana et al., 2007). Additionally, one 'AND' gate was drawn around the splenium of the corpus callosum on the mid-sagittal slice (Fig. 1F).

Automated longitudinal intra-subject analysis (ALISA)

The automated longitudinal intra-subject analysis (ALISA) approach proposed in this work computes for each subject the FT results of the data sets, acquired at *multiple* time points, by defining a *single* ROI configuration on a subject-specific DTI template. The ROI configuration is subsequently applied to each of the individual data sets to obtain the FT results for that subject at each time point. The subject-specific DTI template is created for each subject separately by averaging the multiple diffusion tensor data sets as described previously (Jones et al., 2002) using elastix (Klein et al., 2010). A flow chart illustrating the difference between the manual and ALISA approaches is shown in Fig. 2. In this step of the ALISA approach, the effects of brain growth (both global and/or local) and geometric variations due to acquisition imperfections are assumed to be negligible compared to the precision with which the ROI configurations for tract segmentation can be defined, which is typically in the order of magnitude of a few voxels. To verify that the assumption of spatial correspondence of the reconstructed tracts (or segments thereof) between the different time points holds, non-linear deformation fields have been computed between the DTI data at time points one and five for each of the ten

subjects (Van Hecke et al., 2007). With these deformation fields inter-scan geometric differences and brain growth can be quantified for each voxel. The FA skeletonization procedure of TBSS (Smith et al., 2006) with an FA threshold of 0.2 is used on a representative subject's template to assess the magnitude of these deformation fields overlaid on the main WM fiber pathways.

Performance of ALISA in terms of accuracy and precision is compared to (i) the manual FT segmentations, where ROIs were drawn manually for each bundle at every time points for all subjects; and (ii) an automated *inter-subject* analysis, where FT segmentations were obtained over all time points *and* all subjects as described in Lebel et al. (2008). For this approach – in the following referred to as the "fully automated" method – the DTI atlas was constructed from the ten repeats of the single subject (Jones et al., 2002) and ROI configurations were defined on this atlas for each WM fiber bundle and subsequently applied to the data of *all* time points of *all* subjects (Lebel et al., 2008). For each tractography result from ALISA, the fully automated method, and the bronze standard (i.e., the manual FT segmentations), the FA, MD, RD, AD, and volume were estimated as in Jones et al. (2005a).

Statistical inference

With the ten repeated DTI scans of a single subject, the precision of the aforementioned measures can be compared between the manual, ALISA, and fully automated method. More specifically, using Levene's test (assessing equality of variances) we can determine whether ALISA or the fully automated method would introduce an additional amount of variability to the FT segmentations. In addition, the paired Kruskal–Wallis test was applied to assess any change in accuracy (a non-parametric test is preferred to avoid sensitivity to non-normal data distributions (Kitchen, 2009)). In other words, this paired test will allow us to investigate the existence of any systematic deviation of the estimated measures between the three methods.

For the longitudinal data sets (ten subjects scanned at five time points), a two-way repeated measures ANOVA was applied to investigate potential differences in accuracy between the manual, ALISA, and fully automated approaches if data were normally distributed (as determined with the Lilliefors test with $p = 0.05$ deemed significant) and with the nonparametric Friedman test otherwise. As these are pair-wise statistical
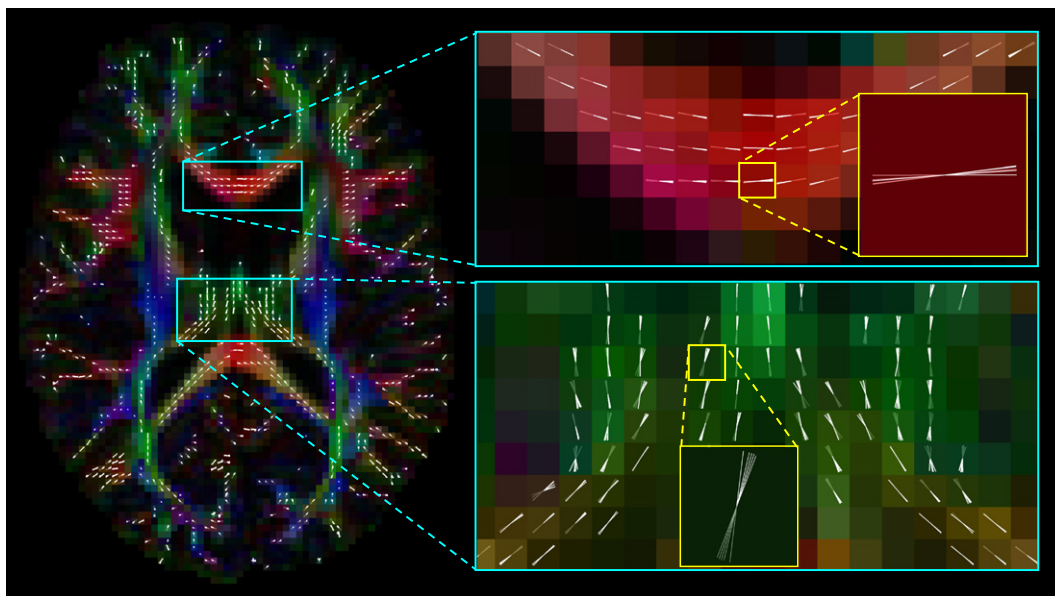
Fig. 4. Directionally color-encoded fractional anisotropy (FA) map of a subject-specific template (derived from the same representative subject shown in Fig. 3) with the principal diffusion orientations (white lines) of each time point overlaid on the corresponding FA skeleton of this template. The enlarged regions-of-interest clearly demonstrate the tight coherence in diffusion orientation across the different time points.

tests between different segmentation methods, these tests provide a very high sensitivity. To assess whether both approaches have a difference in precision based on these longitudinal data sets, the estimated FA, MD, AD, RD, and tract volume values were first adjusted to account for inter-subject differences. More specifically, for each subject and for each reconstructed fiber bundle the average value across the five time points was subtracted from each of the individual time point estimates for all

approaches before performing Levene's test. Differences were deemed significant at $p = 4.76e{-}4$ (Bonferroni corrected for multiple hypothesis testing).

Lastly, we compared the intra-subject variation in segmented tract volumes between the manual, ALISA, and fully automated methods. More specifically, for each subject and the four fiber bundles, the standard deviation of the fiber bundle volume across the five time
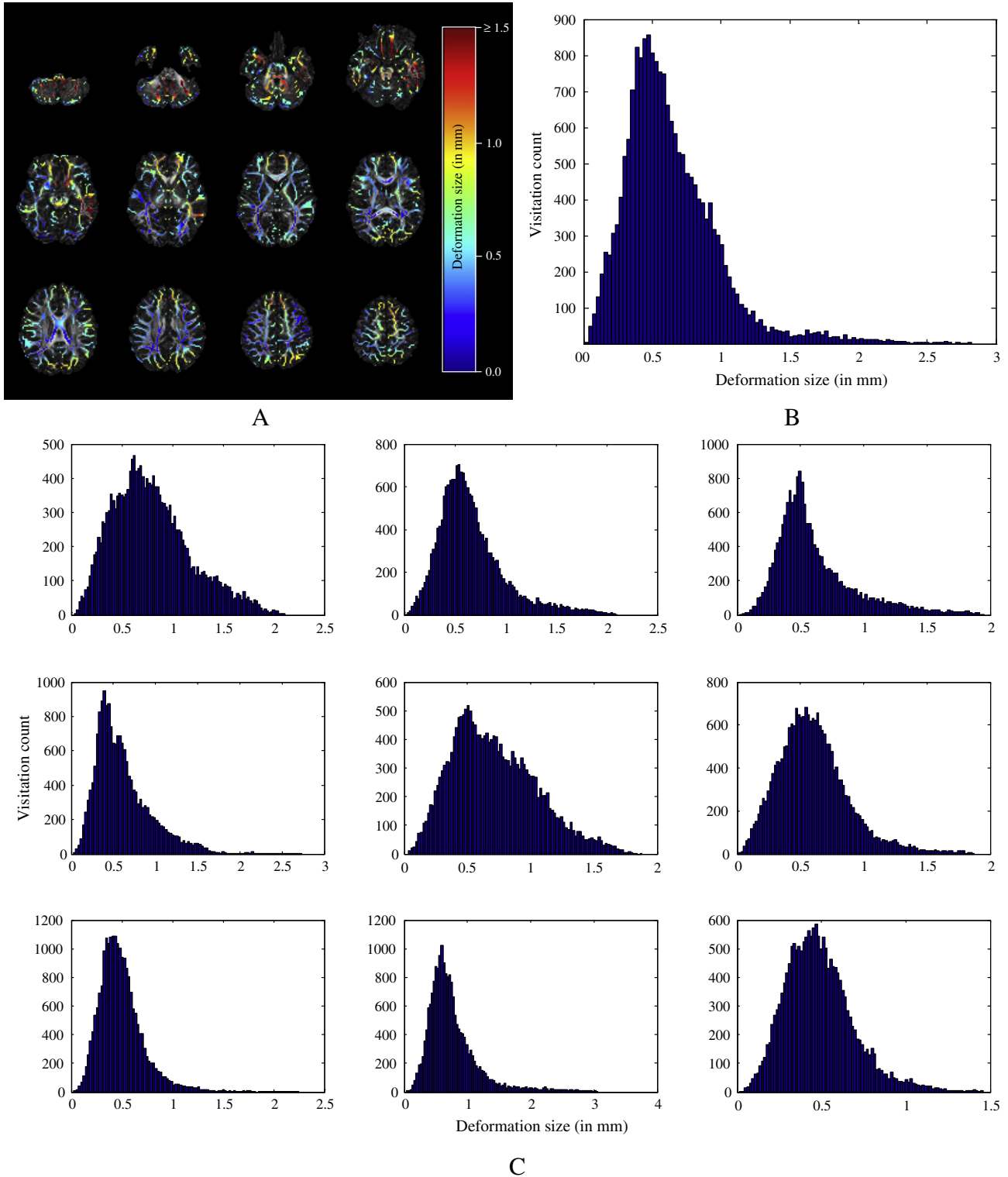
Fig. 5. Magnitude of the voxel-wise displacement field between time points one and five for a representative subject overlaid on the FA skeleton associated with time point five (A). The corresponding distribution of the deformation values shown in (A) is displayed in (B). Histograms of the deformation fields between time points one and five for the other nine subjects are shown in (C). Note that y-axis scales differ to allow comparison of individual distribution.
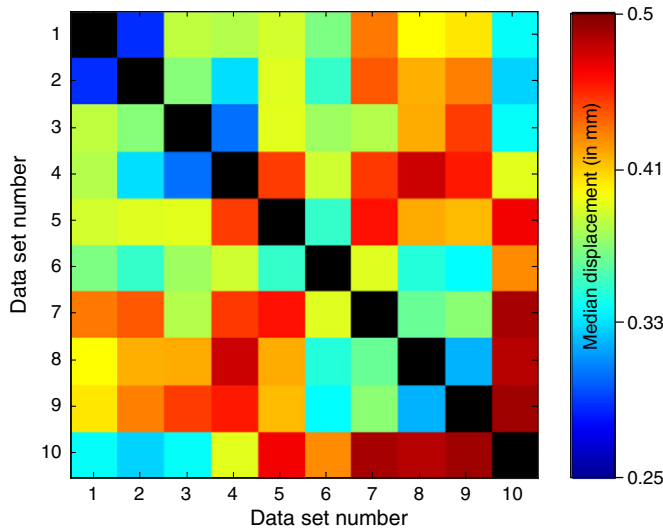
Fig. 6. Median values of the displacement fields between each pair of the ten repeated DTI data acquisitions of the control subject. The black diagonal elements are zero by definition.

points was computed and compared between these methods using Friedman's test.

Results

Subject-specific template construction

The reliability of automating fiber tractography segmentations for serial DTI data depends heavily on the coregistration quality and, consequently, the construction of the subject-specific template that

was used in the ALISA approach. Indicating the quality of the applied normalization procedure (Jones et al., 2002), Fig. 3 shows the resulting template derived from the five serial DTI scans of a representative subject. Overlaid on the FA skeleton of this template, the dominant diffusion direction (first eigenvector) is shown for each individual DTI data set in Fig. 4. The tight coherence of these principal diffusion orientations demonstrates the high level of accuracy that was obtained for our coregistration results.

The magnitude of the non-rigid geometric deformation between time points one and five is shown in Fig. 5A for a representative subject (female, 7.6 year at first scan) with Fig. 5B showing the corresponding histogram of these deformation values. Fig. 5C presents the same histograms of deformation values for the other nine subjects. Notice that virtually all deformations related to brain growth and/or differences in acquisition geometry are smaller than the voxel size. The same procedure was also applied to the ten repeated acquisitions of the single subject to investigate the magnitude of the deformations related to imperfections of the data acquisition in the absence of brain growth. More specifically, each of the ten repeated data sets is registered to every other data set with the corresponding warp fields summarized by their median displacement (see Fig. 6). The average inter-scan deformation magnitude (mean 0.40 ± 0.05 mm) is significantly smaller (independent two-sample t-test; $p < 10^{-10}$) than the deformations between time points one and five of the ten subjects (mean 0.58 ± 0.09 mm).

Ten repeated DTI acquisitions of one control subject

The FA, MD, RD, AD, and volume measures for each of these reconstructed fiber tracts (averaged across the ten repeated scans) are summarized in Table 1. Levene's test and the Kruskal–Wallis test were applied to investigate for each fiber bundle the difference in precision and accuracy of the estimated measures, respectively. As shown in

Table 1
Comparison of DTI metrics and tract volumes of the four fiber bundles across ten repeated DTI acquisitions of a single subject (female, 12.2 years) between the manual FT segmentation, ALISA, and the fully automated (shortened to "full" in the table) method. Values shown are average ± standard deviation.

| | | FA | | Diffusivity ($10^{-3} \times$ mm²/s) | | | | | | | | Volume (cm³) | |
				MD		AD		RD					
SSCing-L	Manual	0.55 ± 0.02	$p_{KW} = 0.99$	0.73 ± 0.01	$p_{KW} = 1$	1.24 ± 0.03	$p_{KW} = 1$	0.47 ± 0.02	$p_{KW} = 0.99$			1.50 ± 0.12	$p_{KW} = 0.80$
	ALISA	0.55 ± 0.02	$p_L = 1$	0.73 ± 0.01	$p_L = 0.98$	1.24 ± 0.03	$p_L = 1$	0.47 ± 0.02	$p_L = 1$			1.49 ± 0.12	$p_L = 0.95$
	Full	0.55 ± 0.02		0.73 ± 0.01		1.24 ± 0.03		0.47 ± 0.02				1.52 ± 0.13	
SSCing-R	Manual	0.52 ± 0.02	$p_{KW} = 0.99$	0.75 ± 0.01	$p_{KW} = 0.98$	1.24 ± 0.02	$p_{KW} = 0.99$	0.51 ± 0.02	$p_{KW} = 0.99$			1.38 ± 0.18	$p_{KW} = 0.94$
	ALISA	0.52 ± 0.02	$p_L = 1$	0.75 ± 0.01	$p_L = 0.99$	1.24 ± 0.02	$p_L = 1$	0.51 ± 0.02	$p_L = 1$			1.35 ± 0.17	$p_L = 0.97$
	Full	0.52 ± 0.02		0.75 ± 0.01		1.24 ± 0.02		0.51 ± 0.02				1.35 ± 0.17	
CST-L	Manual	0.58 ± 0.01	$p_{KW} = 0.18$	0.71 ± 0.01	$p_{KW} = 0.87$	1.25 ± 0.02	$p_{KW} = 0.47$	0.44 ± 0.01	$p_{KW} = 0.18$			9.33 ± 1.23	$p_{KW} = 0.32$
	ALISA	0.59 ± 0.01	$p_L = 0.09$	0.71 ± 0.01	$p_L = 0.69$	1.26 ± 0.02	$p_L = 0.99$	0.43 ± 0.01	$p_L = 0.21$			8.70 ± 0.68	$p_L = 0.10$
	Full	0.59 ± 0.01		0.71 ± 0.01		1.26 ± 0.02		0.43 ± 0.01				8.70 ± 0.68	
CST-R	Manual	0.54 ± 0.01	$p_{KW} = 0.82$	0.73 ± 0.01	$p_{KW} = 0.94$	1.23 ± 0.01	$p_{KW} = 0.83$	0.48 ± 0.01	$p_{KW} = 0.73$			13.05 ± 0.86	$p_{KW} = 7e\text{-}3$
	ALISA	0.54 ± 0.01	$p_L = 0.91$	0.73 ± 0.01	$p_L = 1$	1.23 ± 0.01	$p_L = 0.99$	0.48 ± 0.01	$p_L = 0.83$			11.83 ± 0.60	$p_L = 0.32$
	Full	0.54 ± 0.01		0.73 ± 0.01		1.23 ± 0.01		0.48 ± 0.01				11.83 ± 0.60	
UF-L	Manual	0.40 ± 0.01	$p_{KW} = 1$	0.80 ± 0.02	$p_{KW} = 1$	1.18 ± 0.02	$p_{KW} = 0.98$	0.62 ± 0.01	$p_{KW} = 1$			6.65 ± 0.85	$p_{KW} = 0.95$
	ALISA	0.40 ± 0.01	$p_L = 1$	0.80 ± 0.02	$p_L = 1$	1.18 ± 0.02	$p_L = 1$	0.62 ± 0.01	$p_L = 1$			6.67 ± 0.82	$p_L = 0.59$
	Full	0.40 ± 0.01		0.80 ± 0.02		1.18 ± 0.02		0.62 ± 0.01				6.68 ± 1.01	
UF-R	Manual	0.41 ± 0.01	$p_{KW} = 0.94$	0.81 ± 0.01	$p_{KW} = 1$	1.21 ± 0.02	$p_{KW} = 0.99$	0.62 ± 0.01	$p_{KW} = 0.99$			7.97 ± 0.88	$p_{KW} = 0.72$
	ALISA	0.41 ± 0.01	$p_L = 1$	0.81 ± 0.01	$p_L = 0.99$	1.21 ± 0.02	$p_L = 1$	0.62 ± 0.01	$p_L = 0.99$			8.01 ± 0.82	$p_L = 0.93$
	Full	0.41 ± 0.01		0.81 ± 0.01		1.21 ± 0.02		0.62 ± 0.01				8.26 ± 0.90	
FM	Manual	0.61 ± 0.01	$p_{KW} = 0.18$	0.81 ± 0.01	$p_{KW} = 0.39$	1.48 ± 0.03	$p_{KW} = 0.97$	0.48 ± 0.01	$p_{KW} = 0.28$			8.63 ± 3.02	$p_{KW} = 0.33$
	ALISA	0.60 ± 0.02	$p_L = 0.72$	0.82 ± 0.02	$p_L = 0.37$	1.48 ± 0.02	$p_L = 0.31$	0.49 ± 0.03	$p_L = 0.34$			7.07 ± 0.46	$p_L = 0.06$
	Full	0.60 ± 0.02		0.82 ± 0.02		1.48 ± 0.02		0.49 ± 0.03				7.07 ± 0.46	

FA = fractional anisotropy; MD = mean diffusivity; AD = axial diffusivity; RD = radial diffusivity; SD = standard deviation; SSCing-L/R = left/right superior segment of the cingulum; CST-L/R = left/right cortico-spinal tracts; UF-L/R = left/right uncinate fasciculus; FM = forceps major; ALISA = automated longitudinal intra-subject analysis; p_{KW} = p-value of Kruskal–Wallis test; p_L = p-value of Levene's test. No comparisons were significant at $p = 4.76e - 4$ (Bonferroni corrected). If the comparison yielded a significant effect, post-hoc analyses were performed. Mean values of methods that are significantly different from the other(s) in these post-hoc tests are shown in bold.
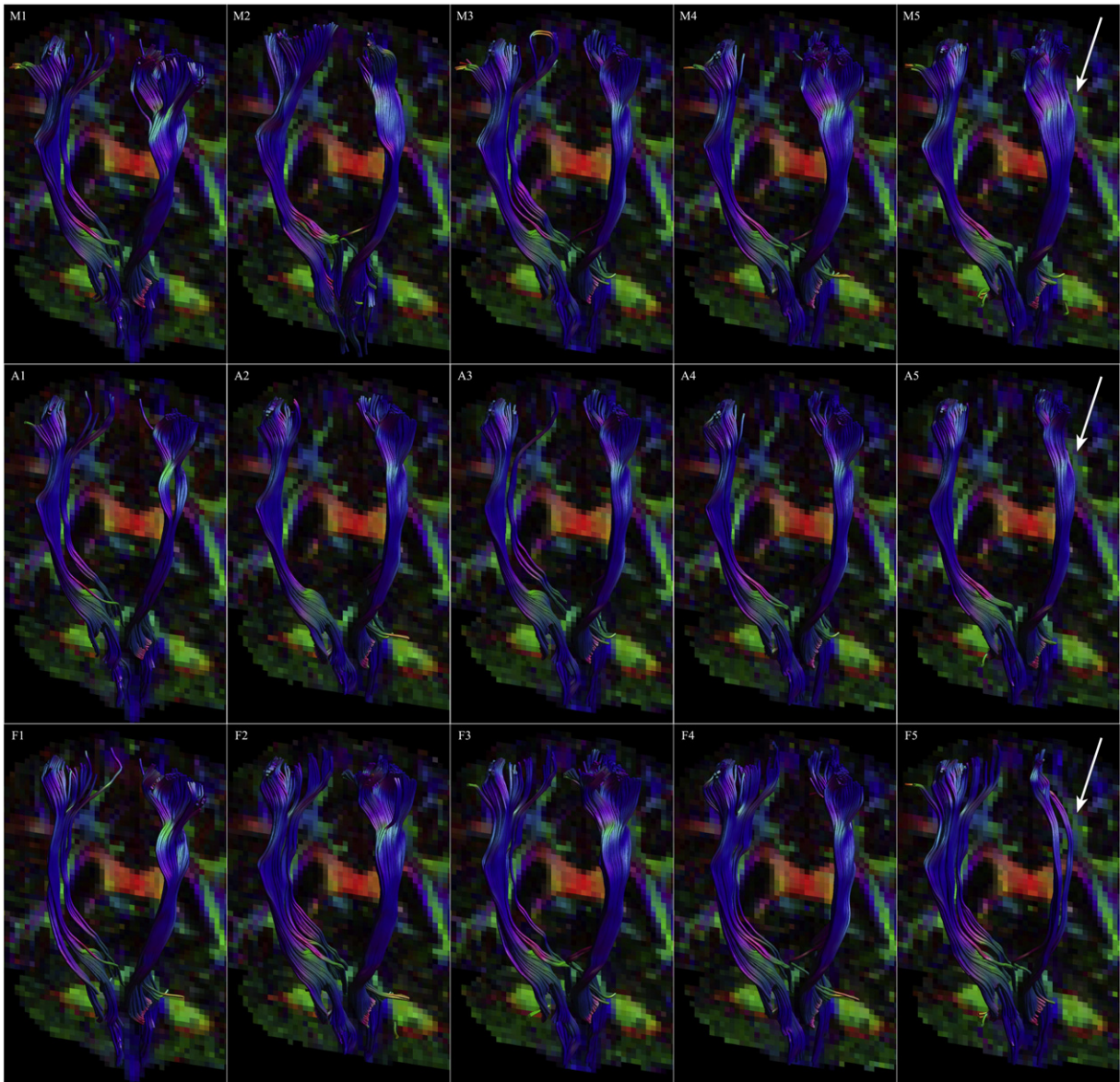
Fig. 7. Segmentations of the bilateral cortico-spinal tracts (CST) for a representative subject (5 time points with 1/2 year intervals), using the manual FT segmentation (M1–M5), ALISA (A1–A5), and the fully automated method (F1–F5). The white arrows indicate the reduced number of tracts in the fully automated segmentations compared to the manual and ALISA methods.

Table 1, no significant differences were observed in either volume or diffusion measures.

Longitudinal data sets (ten subjects scanned five times at six-month intervals)

Figs. 7–10 show the reconstructed pathways of the CST, UF, SSCing, and FM, respectively, of a representative subject at each of the five time points and for the three approaches. Notice that the fiber tracking results obtained with ALISA are almost identical to the manually segmented fiber bundles, but that the fully automated approach shows larger variations, mostly in the SSCing, UF, and FM. Supplementary online material shows the segmented bundles for the other subjects, giving a good overview of inter-subject variability in FT segmentations. Table 2 summarizes the mean and standard deviation of the diffusion metrics (FA, MD, RD, AD) and volume measures of the four fiber bundles across the ten subjects that were scanned five times at roughly six-month intervals (i.e., total number of DTI data sets is 50). The only significant difference in variance was for the FM volume, which was different when segmented with the fully automated method compared to ALISA and the manual FT segmentations. In addition, significant differences across the three approaches were observed in mean values for the volume and several diffusion indices of the bilateral CST. The most striking difference is the reduced number of tracts in the left CST for the fully automated method (white arrow in Fig. 7). More subtle differences between the three segmentation approaches can be observed in the extent with which the tracts terminate in superior and/or inferior regions.

The intra-subject standard deviation of the fiber bundle volume across the five time points is significantly different between the three methods ($p = 2e-6$) if all fiber bundles are pooled together. Table 3 shows the results of such comparison for each fiber bundle separately, with ALISA providing the lowest standard deviations, indicating the highest intra-subject consistency in fiber bundle volumes.

Discussion

With the advent of large-cohort DTI studies, there is an increased demand for data analyses that require minimal user input. While several methods have been developed to analyze WM fiber bundles in
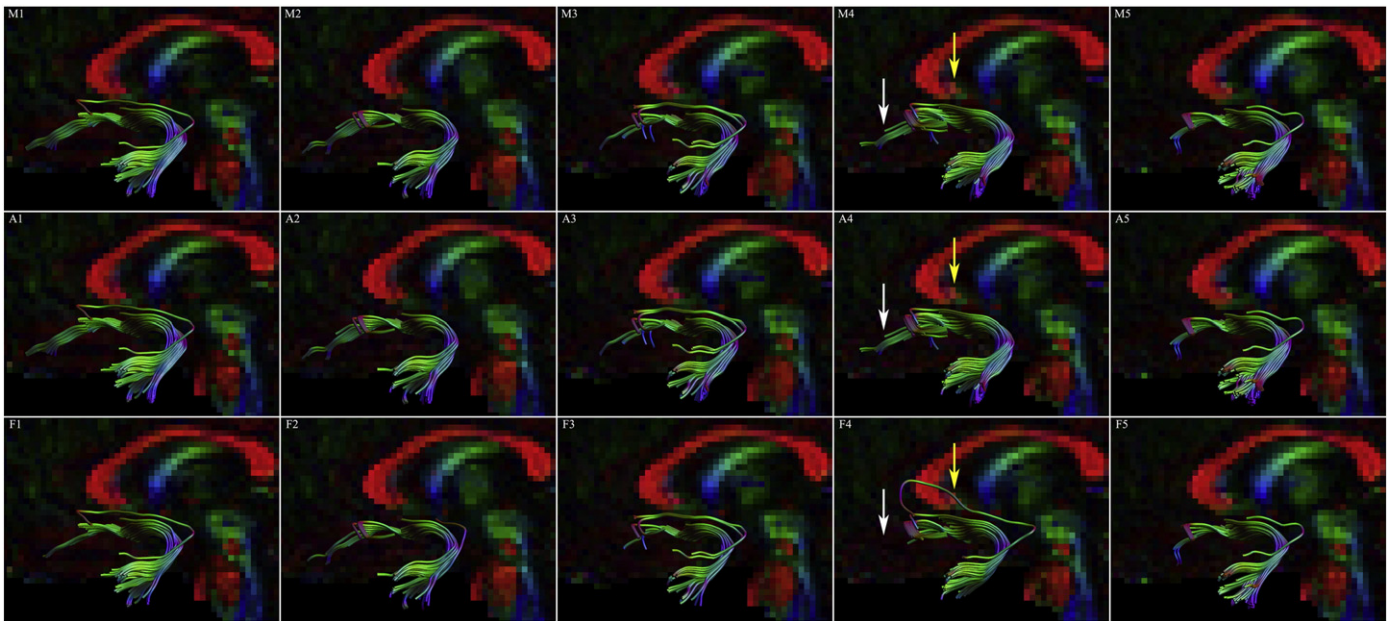
Fig. 8. Segmentations of the uncinate fasciculus (left hemisphere) for a representative subject (5 time points with 1/2 year intervals), using the manual FT segmentation (M1–M5), ALISA (A1–A5), and the fully automated method (F1–F5). Notice the larger variability between time points in the frontal projections in the fully automated segmentation, most notably in F4, that is not present for manual or ALISA segmentations (white arrows). The yellow arrows indicate an erroneous tract in F4 that is not present in M4 or A4.

an automated way (Clayden et al., 2007; Hagler et al., 2009; Lebel et al., 2008; Leemans et al., 2006; O'Donnell et al., 2009; Reich et al., 2010; Suarez et al., 2012; Verhoeven et al., 2010; Yendiki et al., 2011; Zhang et al., 2010), there is typically a trade-off that needs to be made between

prior knowledge incorporated by the user for the manual approach (e.g., the neuroanatomical expertise regarding the location and extent of tracts-of-interests) and the predefined parameter settings required by the automated technique. In other words, the labor-intensive and
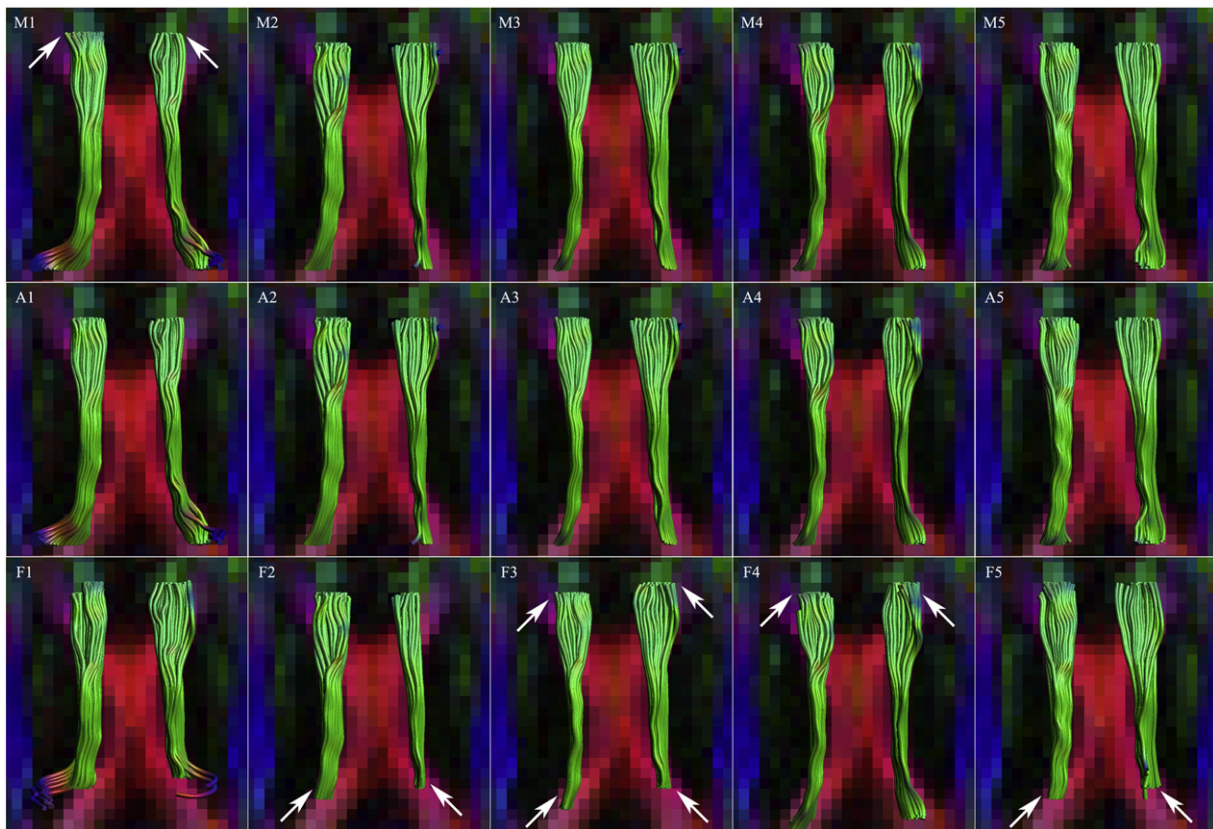
Fig. 9. Segmentations of the cingulum segments for a representative subject (5 time points with 1/2 year intervals), using the manual FT segmentation (M1–M5), ALISA (A1–A5), and the fully automated method (F1–F5). Notice the difference in location of the ROIs that were used to define the boundaries of the cingulum segments between M1 and M2–M5, and more severely between the different fully automated segmentations (as indicated with the white arrows).
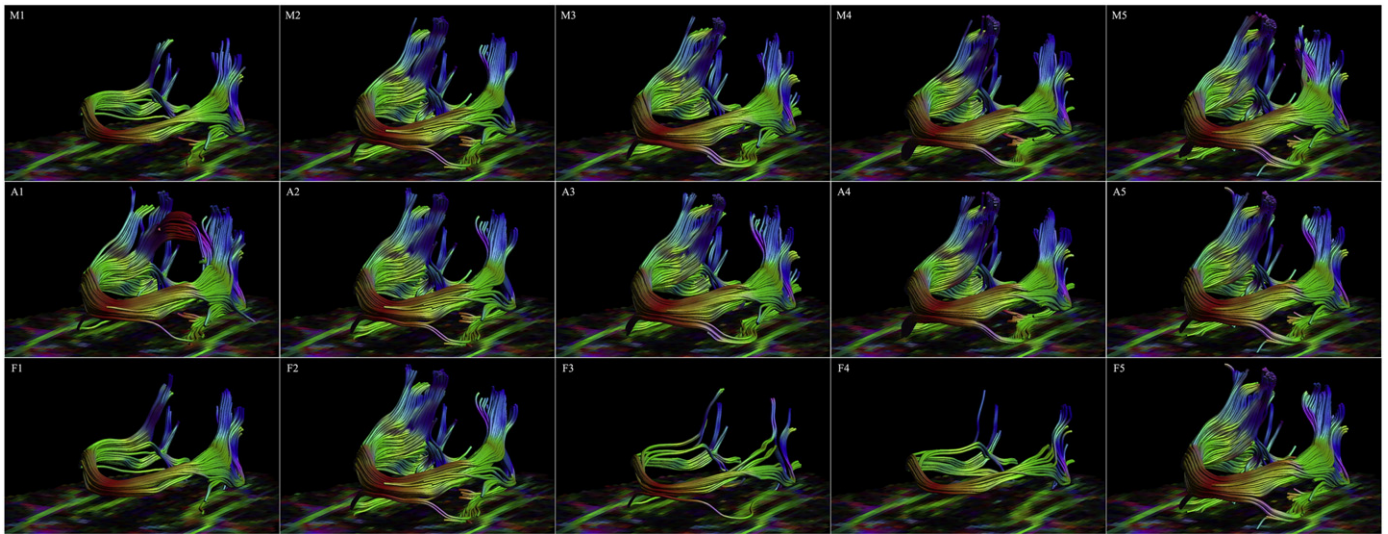
Fig. 10. Segmentations of forceps major (FM) for a representative subject (5 time points with 1/2 year intervals), using the manual FT segmentation (M1–M5), ALISA (A1–A5), and the fully automated method (F1–F5). For the fully automated method, there is a large variability in the segmented tracts between the different time points, most notably when comparing F2 and F5 to F3 and F4. The manual and ALISA methods show more consistent and stable tract segmentations.

subjective – yet valuable – human input is exchanged with the higher objectivity and efficiency, but potentially the lower accuracy, of the automated analysis tool.

In this paper, we have proposed a new analysis pipeline, dubbed ALISA, which aims to combine the best of both worlds: increasing the efficiency by automating the subject-specific data analysis, while retaining the prior knowledge from the neuroanatomical expert on a subject-by-subject basis. In addition, we have evaluated the performance of the ALISA approach by comparing its reliability in terms of accuracy and precision with the current "bronze standard", i.e., with the corresponding manual FT segmentations. Furthermore, we have investigated whether an existing fully-automated *inter-subject* segmentation approach (Lebel et al., 2008) would give the same accuracy and precision as ALISA and/or the manual FT segmentations. To this end, FT segmentations and several diffusion measures from four different fiber bundles (SSCing, CST, UF, and FM) were compared

Table 2

Comparison of DTI metrics and tract volumes of the four fiber bundles across ten different subjects scanned at 5 time points (1/2 year intervals) between the manual FT segmentation, ALISA, and the fully automated (shortened to "full" in the table) method. Values shown are average ± standard deviation.

		FA		Diffusivity ($10^{-3} \times mm^2/s$)						Volume (cm^3)	
				MD		AD		RD			
SSCing-L	Manual	0.52 ± 0.04	$p_A = 0.20$	0.75 ± 0.02	$p_A = 0.49$	1.23 ± 0.06	$p_F = 0.24$	0.51 ± 0.03	$p_A = 0.71$	1.52 ± 0.37	$p_F = 0.60$
	ALISA	0.52 ± 0.04	$p_L = 0.96$	0.75 ± 0.02	$p_L = 1$	1.23 ± 0.06	$p_L = 0.74$	0.51 ± 0.03	$p_L = 0.86$	1.53 ± 0.44	$p_L = 0.04$
	Full	0.52 ± 0.04		0.75 ± 0.02		1.23 ± 0.06		0.51 ± 0.03		1.62 ± 0.68	
SSCing-R	Manual	0.46 ± 0.05	$p_F = 0.53$	0.79 ± 0.03	$p_A = 0.04$	1.22 ± 0.06	$p_F = 0.20$	0.57 ± 0.04	$p_A = 0.02$	1.29 ± 0.41	$\mathbf{p_F = 1e-5}$
	ALISA	0.46 ± 0.04	$p_L = 0.94$	0.79 ± 0.03	$p_L = 0.87$	1.22 ± 0.06	$p_L = 0.73$	0.57 ± 0.04	$p_L = 0.97$	1.32 ± 0.46	$p_L = 0.20$
	Full	0.46 ± 0.04		0.79 ± 0.03		1.22 ± 0.05		0.57 ± 0.04		$\mathbf{1.49 \pm 0.57}$	
CST-L	Manual	0.54 ± 0.02	$p_A = 0.46$	0.73 ± 0.02	$p_F = 0.22$	1.22 ± 0.03	$p_F = 5e-4$	0.48 ± 0.02	$p_A = 0.98$	$\mathbf{8.08 \pm 1.94}$	$\mathbf{p_A = 3e-4}$
	ALISA	0.54 ± 0.02	$p_L = 0.96$	0.73 ± 0.02	$p_L = 0.96$	1.23 ± 0.03	$p_L = 0.91$	0.48 ± 0.02	$p_L = 0.92$	7.10 ± 1.97	$p_L = 0.11$
	Full	0.54 ± 0.02		0.73 ± 0.02		1.22 ± 0.03		0.48 ± 0.02		7.64 ± 2.22	
CST-R	Manual	$\mathbf{0.53 \pm 0.02}$	$\mathbf{p_A = 1e-4}$	0.74 ± 0.02	$\mathbf{p_A = 1e-11}$	1.24 ± 0.03	$p_A = 0.10$	$\mathbf{0.50 \pm 0.02}$	$\mathbf{p_A = 7e-8}$	7.71 ± 2.05	$\mathbf{p_A = 2e-8}$
	ALISA	$\mathbf{0.53 \pm 0.02}$	$p_L = 0.45$	0.74 ± 0.02	$p_L = 0.13$	1.24 ± 0.03	$p_L = 0.46$	$\mathbf{0.49 \pm 0.02}$	$p_L = 0.05$	7.30 ± 2.06	$p_L = 0.09$
	Full	$\mathbf{0.52 \pm 0.02}$		$\mathbf{0.75 \pm 0.02}$		1.25 ± 0.03		$\mathbf{0.50 \pm 0.02}$		8.66 ± 2.45	
UF-L	Manual	0.39 ± 0.01	$p_A = 0.63$	0.84 ± 0.02	$p_A = 0.09$	1.23 ± 0.02	$p_F = 0.62$	0.65 ± 0.02	$p_A = 0.12$	4.73 ± 1.16	$p_F = 0.51$
	ALISA	0.39 ± 0.01	$p_L = 0.58$	0.84 ± 0.02	$p_L = 0.26$	1.23 ± 0.02	$p_L = 0.18$	0.65 ± 0.02	$p_L = 0.40$	4.83 ± 1.25	$\mathbf{p_L = 2e-4}$
	Full	0.39 ± 0.01		0.85 ± 0.02		1.23 ± 0.03		0.65 ± 0.02		$\mathbf{4.83 \pm 1.71}$	
UF-R	Manual	0.39 ± 0.01	$\mathbf{p_A = 9e-5}$	0.83 ± 0.02	$p_A = 0.13$	1.21 ± 0.03	$p_A = 0.18$	0.64 ± 0.02	$p_A = 4e-3$	5.37 ± 1.74	$p_A = 0.02$
	ALISA	0.39 ± 0.01	$p_L = 0.40$	0.83 ± 0.02	$p_L = 0.62$	1.21 ± 0.03	$p_L = 0.72$	0.64 ± 0.02	$p_L = 0.54$	5.27 ± 1.73	$p_L = 0.01$
	Full	$\mathbf{0.39 \pm 0.01}$		0.83 ± 0.02		1.21 ± 0.02		0.65 ± 0.02		5.08 ± 1.87	
FM	Manual	0.60 ± 0.03	$p_F = 3e-3$	0.82 ± 0.05	$p_A = 8e-3$	1.47 ± 0.06	$p_F = 0.59$	0.49 ± 0.05	$p_A = 7e-4$	9.97 ± 2.91	$\mathbf{P_A = 2e-20}$
	ALISA	0.60 ± 0.03	$p_L = 3e-3$	0.81 ± 0.04	$p_L = 0.04$	1.47 ± 0.06	$p_L = 0.02$	0.48 ± 0.04	$p_L = 0.04$	10.33 ± 2.97	$\mathbf{p_L = 3e-4}$
	Full	0.59 ± 0.04		0.83 ± 0.05		1.48 ± 0.07		0.51 ± 0.06		$\mathbf{5.61 \pm 2.01}$	

FA = fractional anisotropy; MD = mean diffusivity; AD = axial diffusivity; RD = radial diffusivity; SD = standard deviation; SSCing-L/R = left/right superior segment of the cingulum; CST-L/R = left/right cortico-spinal tracts; UF-L/R = left/right uncinate fasciculus; FM = forceps major; ALISA = automated longitudinal intra-subject analysis; p_L = p-value of Levene's test (Levene's test was performed on the adjusted data values that take the inter-subject variation into account); p_A = p-value of parametric repeated-measures ANOVA; p_F = p-value of non-parametric Friedman test (in case non-normality of the data or unequal variances were observed as determined with the Lilliefors or Levene's test, respectively). The p-values shown in bold are significant at $p = 4.76e-4$ (Bonferroni corrected). If the comparison yielded a significant effect, post-hoc analyses were performed. Mean values of methods that are significantly different from the other(s) in these post-hoc tests are shown in bold.

Table 3
Comparison of the intra-subject standard deviation of the tract volume across the five time points between the manual FT segmentation, ALISA, and the fully automated method (the presented values are the average over all ten subjects, in cm^3).

	SSCing-L	SSCing-R	CST-L	CST-R	UF-L	UF-R	FM
Manual	0.16	0.17	1.08	1.14	0.62	0.71	2.57
ALISA	0.16	0.16	0.93	1.03	0.60	0.65	1.01
Fully automated	0.29	0.23	1.49	1.61	1.00	**1.01**	1.36
Friedman's test	$p = 0.067$	$p = 0.061$	$p = 0.301$	$p = 0.273$	$p = 0.045$	**$p = 0.007$**	$p = 0.014$

SSCing-L/R = left/right superior segment of the cingulum; CST-L/R = left/right cortico-spinal tracts; UF-L/R = left/right uncinate fasciculus; FM = forceps major; ALISA = automated longitudinal intra-subject analysis. The p-values shown in bold are significant at $p = 0.007$ (Bonferroni corrected). If Friedman's test between all methods yielded a significant result, post-hoc analyses were performed. Methods that are significantly different from the others in these post-hoc tests have the values shown in bold.

between all three methods using (i) ten repeated data sets of a single subject, where no detectable brain changes were assumed and (ii) five serial acquisitions (half a year apart) for ten different subjects, which are all part of the HUBU cohort database ("Hjernens Udvikling hos Børn og Unge": Brain maturation in children and adolescents; see Madsen et al., 2010, 2011). ALISA will be made available via the *ExploreDTI* diffusion MRI software tool (www.exploredti.com).

The ALISA method had the smallest intra-subject variability in the organization of the fiber bundles compared to the fully automated method and the manual FT segmentation (Figs. 7–10 and Table 3), especially in the SSCing, UF, and FM. For the SSCing, for instance, where the aim was to extract only the segment between the ROIs, there is a strong variability in the length of this segment when extracted with the fully automated method (Fig. 9). This is also supported by a significant difference in variance of the segmented tract volume between the fully automated method on the one hand and the ALISA and manual segmentation on the other hand. Similarly, the tract volumes of the FM are also significantly different when segmented with the fully automated method (Table 2). In addition, the variability between the segmented FM tracts from the five time points of one subject is much larger for the fully automated method (Fig. 10). Most notably, the fully automated method was unable to segment the FM on one time points from one subject (Supplementary material — subj. 7). Furthermore, the UF segmented with the fully automated method is prone to missing the frontal projections (Fig. 8) or the temporal projections (Supplementary material - subj.2 and 6). Based on these results of the longitudinal datasets, one can already state that the fully automated method does not give the same high level of reliability as the manual FT segmentations. By contrast, the ALISA method shows results that are more consistent with the manual segmentations, indicating that the same regions have been investigated.

Despite the absence of any significant differences between the ALISA and manual results for the ten repeated data sets, there is a tendency towards higher variability with the manual approach, which can be appreciated from its slightly higher overall standard deviation in tract volume estimates (Table 1). This trend in higher variability for manual segmentations can be attributed to the different ROI positions that were used to extract the tracts-of-interest for each data set separately (Supplementary Figs. S1–S4), which can also be appreciated in the tract segmentations in the longitudinal dataset (Fig. 9). These differences in position, which by design are not present in the ALISA framework, are probably caused by the intrinsic intra-rater variability triggered by subtle differences in partial volume effects and noise distributions across the ten data sets. Also for the five serial acquisitions from ten subjects, no significant differences in accuracy/precision of the diffusion measures between both approaches could be detected, suggesting that ALISA does not affect the precision and accuracy in an adverse way. One could argue that the higher SNR in the subject-specific templates could increase the consistency of the ROI delineations across subjects, making the ALISA approach more robust and efficient than manual delineations, especially for large-cohort studies. This consideration is supported by Table 3 demonstrating that ALISA has lower intra-subject variation in segmented tract volumes than the manual segmentations.

There is no significant difference in precision of the diffusivity and volume measures between manual FT segmentation and ALISA, as determined using Levene's test (Tables 1 and 2). Table 2 further shows the minute differences in the average diffusion values between the manual and ALISA approaches. Taken together, these results indicate that the absolute values of these measures will be slightly different when using either the manual or ALISA segmentations, but the statistical power to detect any trends or changes would remain the same, or potentially higher with ALISA due to higher intra-subject consistency in tract segmentation (Table 3, Figs. 7–10).

The ALISA approach assumes that the position of the ROI – defined on the subject-specific template – can be transformed to the same anatomical locations across different time points. This assumption holds if brain growth can be considered to be in the order of magnitude of the precision with which one can draw the ROI, so in the order of the voxel size. Although brain growth could indeed be verified by the larger median displacements of the deformation warp fields observed in the serial data sets (see Subject-specific template construction section), the vast majority of voxels did not exceed 2 mm (Fig. 5). Also qualitatively, the validity of the assumption could already be appreciated from the high spatial agreement between the five normalized DTI data sets for the representative subject shown in Figs. 3 and 4 (Jones et al., 2002). In general brain size is relatively stable between 6–7 and 70 years of age (e.g., Dekaban, 1978; Jernigan et al., 2011). We therefore believe that the ALISA approach is suitable for a large range of ages and time spans between first and last scan point.

Nevertheless, in severe pathological conditions (Nimsky et al., 2005, 2006), correspondence between anatomically identical locations may not be warranted, which could be problematic for the ALISA approach. Similar complications may arise in neonatology related research (Van der Aa et al., 2011), where there can be tremendous changes in brain size and WM organization between follow-up scans may not be captured by the ALISA framework. Possible improvements might include a nonlinear registration from the template to the individual time points of each subject, but the stability and reproducibility of the nonlinear registration should be carefully monitored to determine whether this yields a benefit because of accurate anatomical correspondence or merely causes additional variability due to imperfect registration.

We evaluated the ALISA framework for four specific WM fiber bundles, and with DTI data sets acquired from healthy young subjects. By including association (SSCing and UF), projection (CST), and commissural (FM) fibers, we cover a wide variety of fiber structures with different sizes and locations. In general, ALISA can also be applied to other WM structures and age ranges as long as the geometric differences across the time points are not too large (i.e., smaller than roughly 5 mm).

Finally, although ALISA has been evaluated with FT segmentations that were based on conventional DTI-based tractography – which nowadays may not be considered as the "optimal" model to perform tract reconstructions (e.g., Jeurissen et al., 2013; Jones et al., 2013) – our proposed framework will also be valid for tractography methods based on other approaches, such as, for instance, diffusion spectrum imaging, Q-ball imaging, and spherical deconvolution methods (Descoteaux et al., 2009; Jeurissen et al., 2011; Wedeen et al., 2008).

In summary, we have proposed and evaluated an automated longitudinal intra-subject analysis, coined ALISA, which is specifically designed to analyze tractography-based segmentations for longitudinally acquired DTI data sets. In contrast to *across-subject* automation, ALISA has comparable to even higher levels of accuracy and precision compared to manual segmentations. Being less time-consuming and more objective, ALISA will be beneficial for longitudinal studies, especially if data sets have been acquired at many time points.

Acknowledgments

Appendix A. Supplementary material

Supplementary data to this article can be found online at http://dx.doi.org/10.1016/j.neuroimage.2013.10.026.

References

Basser, P.J., Mattiello, J., LeBihan, D., 1994. MR diffusion tensor spectroscopy and imaging. Biophys. J. 66 (1), 259–267.

Basser, P.J., Pajevic, S., Pierpaoli, C., Duda, J., Aldroubi, A., 2000. In vivo fiber tractography using DT-MRI data. Magn. Reson. Med. 44 (4), 625–632.

Beaulieu, C., 2002. The basis of anisotropic water diffusion in the nervous system — a technical review. NMR Biomed. 15 (7–8), 435–455.

Caeyenberghs, K., Leemans, A., Geurts, M., Taymans, T., Van der Linden, C., Smits-Engelsman, B.C.M., Sunaert, S., Swinnen, S.P., 2010. Brain-behavior relationships in young traumatic brain injury patients: fractional anisotropy measures are highly correlated with dynamic visuomotor tracking performance. Neuropsychologia 48 (5), 1472–1482.

Catani, M., Thiebaut de Schotten, M., 2008. A diffusion tensor imaging tractography atlas for virtual in vivo dissections. Cortex 44 (8), 1105–1132.

Cercignani, M., 2010. Strategies for Patient–Control Comparison of Diffusion MR Data. In: Jones, D.K. (Ed.), Diffusion MRI. Oxford University, pp. 485–499.

Cercignani, M., Inglese, M., Pagani, E., Comi, G., Filippi, M., 2001. Mean diffusivity and fractional anisotropy histograms of patients with multiple sclerosis. AJNR Am. J. Neuroradiol. 22, 952–958.

Chang, L.C., Jones, D.K., Pierpaoli, C., 2005. RESTORE: robust estimation of tensors by outlier rejection. Magn. Reson. Med. 53 (5), 1088–1095.

Ciccarelli, O., Parker, G.J., Toosy, A.T., Wheeler-Kingshott, C.A., Barker, G.J., Boulby, P.A., Miller, D.H., Thompson, A.J., 2003. From diffusion tractography to quantitative white matter tract measures: a reproducibility study. NeuroImage 18 (2), 348–359.

Ciccarelli, O., Behrens, T.E., Altmann, D.R., Orrell, R.W., Howard, R.S., Johansen-Berg, H., Miller, D.H., Matthews, P.M., Thompson, A.J., 2006. Probabilistic diffusion tractography: a potential tool to assess the rate of disease progression in amyotrophic lateral sclerosis. Brain 129 (7), 1859–1871.

Clark, K.A., Neuchterlein, K.H., Asarnow, R.F., Hamilton, L.S., Phillips, O.R., Hageman, N.S., Woods, R.P., Alger, J.R., Toga, A.W., Narr, K.L., 2011. Mean diffusivity and fractional anisotropy as indicators of disease and genetic liability to schizophrenia. J. Psychiatr. Res. 45 (7), 980–988.

Clayden, J.D., Storkey, A.J., Bastin, M.E., 2007. A probabilistic model-based approach to consistent white matter segmentation. IEEE Trans. Med. Imaging 26 (11), 1555–1561.

Colby, J.B., Soderberg, L., Lebel, C., Dinov, I.D., Thompson, P.M., Sowell, E.R., 2012. Along-tract statistics allow for enhanced tractography analysis. NeuroImage 59 (4), 3227–4242.

Concha, L., Beaulieu, C., Gross, D.W., 2005a. Bilateral limbic diffusion abnormalities in unilateral temporal lobe epilepsy. Ann. Neurol. 57 (2), 188–196.

Concha, L., Gross, D.W., Beaulieu, C., 2005b. Diffusion tensor tractography of the limbic system. AJNR Am. J. Neuroradiol. 26 (9), 2267–2274.

Concha, L., Beaulieu, C., Wheatley, B.M., Gross, D.W., 2007. Bilateral white matter diffusion changes persist after epilepsy surgery. Epilepsia 48 (5), 931–940.

Concha, L., Beaulieu, C., Collins, D.L., Gross, D.W., 2009. White-matter diffusion abnormalities in temporal-lobe epilepsy with and without mesial temporal sclerosis. J. Neurol. Neurosurg. Psychiatry 80 (3), 312–319.

Conturo, T.E., Lori, N.F., Cull, T.S., Akbudak, E., Snyder, A.Z., Shimony, J.S., Mckinstry, R.C., Burton, M., Raichle, M.E., 1999. Tracking neuronal fiber pathways in the living human brain. Proc. Natl. Acad. Sci. U. S. A. 96, 10422–10427.

Cook, P.A., Bai, Y., Nedjati-Gilani, S., Seunarine, K.K., Hall, M.G., Parker, G.J., Alexander, D.C., 2006. Camino: open-source diffusion-MRI reconstruction and processing. 14th Annual Meeting of Intl. Soc. Mag. Reson. Med., Seattle, WA, USA, p. 2759.

Danielian, L.E., Iwata, N.K., Thomasson, D.M., Floeter, M.K., 2010. Reliability of fiber tracking measurements in diffusion tensor imaging for longitudinal study. NeuroImage 49, 1572–1580.

Dekaban, A.S., 1978. Changes in brain weights during the span of human life: relation of brain weights to body heights and body weights. Ann. Neurol. 4 (4), 345–356.

Deprez, S., Amant, F., Yigit, R., Porke, K., Verhoeven, J., Van den Stock, J., Smeets, A., Christiaens, M.R., Leemans, A., Van Hecke, W., Vandenberghe, J., Vandenbulcke, M., Sunaert, S., 2011. Chemotherapy-induced structural changes in cerebral white matter and its correlation with impaired cognitive functioning in breast cancer patients. Hum. Brain Mapp. 32 (3), 480–493.

Deprez, S., Amant, F., Smeets, A., Peeters, R., Leemans, A., Van Hecke, W., Verhoeven, J., Christiaens, M.R., Vandenberghe, J., Vandenbulcke, M., Sunaert, S., 2012. Longitudinal assessment of chemotherapy-induced structural changes in cerebral white matter and its correlation with impaired cognitive functioning. J. Clin. Oncol. 30 (3), 274–281.

Descoteaux, M., Deriche, R., Knosche, T.R., Anwander, A., 2009. Deterministic and probabilistic tractography based on complex fibre orientation distributions. IEEE Trans. Med. Imaging 28 (2), 269–286.

Eluvathingal, T.J., Hasan, K.M., Kramer, L., Fletcher, J.M., Ewing-Cobbs, L., 2007. Quantitative diffusion tensor tractography of association and projection fibers in normally developing children and adolescents. Cereb. Cortex 17 (12), 2760–2768.

Emsell, L., Leemans, A., Langan, C., Barker, G., van der Putten, W., McCarthy, P., Skinner, R., McDonald, C., Cannon, D.M., 2009. A DTI tractography study of the cingulum in euthymic bipolar I disorder. Proceedings of the 17th Annual Meeting of International Society for Magnetic Resonance in Medicine, Hawaii, USA, p. 1224.

Faria, A.V., Hoon, A., Stashinko, E., Li, X., Jiang, H., Mashayekh, A., Akhter, K., Hsu, J., Oishi, K., Zhang, J., Miller, M.I., van Zijl, P.C., Mori, S., 2011. Quantitative analysis of brain pathology based on MRI and brain atlases–applications for cerebral palsy. NeuroImage 54 (3), 1854–1861.

Giorgio, A., Watkins, K.E., Chadwick, M., James, S., Winmill, L., Douaud, G., De Stefano, N., Matthews, P.M., Smith, S.M., Johansen-Berg, H., James, A.C., 2010. Longitudinal changes in grey and white matter during adolescence. NeuroImage 49 (1), 94–103.

Gong, G., Shi, F., Concha, L., Beaulieu, C., Gross, D.W., 2008. Insights into the sequence of structural consequences of convulsive status epilepticus: a longitudinal MRI study. Epilepsia 49 (11), 1941–1945.

Hagler Jr., D.J., Ahmadi, M.E., Kuperman, J., Holland, D., McDonald, C.R., Halgren, E., Dale, A.M., 2009. Automated white-matter tractography using a probabilistic diffusion tensor atlas: application to temporal lobe epilepsy. Hum. Brain Mapp. 30 (5), 1535–1547.

Hagmann, P., Cammoun, L., Gigandet, X., Meuli, R., Honey, C.J., Wedeen, V.J., Sporns, O., 2008. Mapping the structural core of human cerebral cortex. PLoS Biol. 6 (7), e159.

Hasan, K.M., Iftikhar, A., Kamali, A., Kramer, L.A., Ashtari, M., Cirino, P.T., Papanicolaou, A.C., Fletcher, J.M., Ewing-Cobbs, L., 2009. Development and aging of the human brain uncinate fasciculus across the lifespan using diffusion tensor imaging. Brain Res. 1276 (18), 67–76.

Hasan, K.M., Walimuni, S., Abid, H., Hahn, K.R., 2011. A review on diffusion tensor magnetic resonance imaging computational methods and software tools. Comput. Biol. Med. 41 (12), 1062–1072.

Heiervang, E., Behrens, T.E., Mackay, C.E., Robson, M.D., Johansen-Berg, H., 2006. Between session reproducibility and between subject variability of diffusion MR and tractography measures. NeuroImage 33 (3), 867–877.

Hsu, J.L., Leemans, A., Bai, C.H., Lee, C.H., Tsai, Y.F., Chiu, H.C., Chen, W.H., 2008. Gender differences and age-related white matter changes of the human brain: a diffusion tensor imaging study. NeuroImage 39 (2), 566–577.

Hsu, J.L., Van Hecke, W., Bai, C.H., Lee, C.H., Tsai, Y.F., Chiu, H.C., Jaw, F.S., Hsu, C.Y., Leu, J.G., Chen, W.H., Leemans, A., 2010. Microstructural white matter changes in normal aging: a diffusion tensor imaging study with higher-order polynomial regression models. NeuroImage 49 (1), 32–43.

Jansons, K.M., Alexander, D.C., 2003. Persistent angular structure: new insights from diffusion magnetic resonance imaging data. Inverse Prob. 19, 1031–1046.

Jernigan, T.L., Baaré, W.F., Stiles, J., Madsen, K.S., 2011. Postnatal brain development: structural imaging of dynamic neurodevelopment processes. Prog. Brain Res. 189, 77–92.

Jeurissen, B., Leemans, A., Jones, D.K., Tournier, J.D., Sijbers, J., 2011. Probabilistic fiber tracking using the residual bootstrap with constrained spherical deconvolution. Hum. Brain Mapp. 32, 461–479.

Jeurissen, B., Leemans, A., Tournier, J.D., Jones, D.K., Sijbers, J., 2013. Investigating the prevalence of complex fiber configurations in white matter tissue with diffusion magnetic resonance imaging. Hum. Brain Mapp. 34 (11), 2747–2766 http://dx.doi.org/10.1002/hbm.22099.

Johansen-Berg, H., 2010. Behavioural relevance of variation in white matter microstructure. Curr. Opin. Neurol. 23, 351–358.

Jones, D.K., 2008. Studying connections in the living human brain with diffusion MRI. Cortex 44, 936–952.

Jones, D.K., Leemans, A., 2011. Diffusion tensor imaging. Methods Mol. Biol. 711, 127–144.

Jones, D.K., Simmons, A., Williams, S.C.R., Horsfield, M.A., 1999a. Noninvasive assessment of axonal fiber connectivity in the human brain via diffusion tensor MRI. Magn. Reson. Med. 42, 37–41.

Jones, D.K., Horsfield, M.A., Simmons, A., 1999b. Optimal strategies for measuring diffusion in anisotropic systems by MRI. Magn. Reson. Med. 42 (3), 515–525.

Jones, D.K., Griffin, L.D., Alexander, D.C., Catani, M., Horsfield, M.A., Howard, R., Williams, S.C., 2002. Spatial normalization and averaging of diffusion tensor MRI data sets. NeuroImage 17 (2), 592–617.

Jones, D.K., Travis, A.R., Eden, G., Pierpaoli, C., Basser, P.J., 2005a. PASTA: pointwise assessment of streamline tractography attributes. Magn. Reson. Med. 53, 1462–1467.

Jones, D.K., Symms, M.R., Cercignani, M., Howard, R.J., 2005b. The effect of filter size on VBM analyses of DT-MRI data. NeuroImage 26 (2), 546–554.

Jones, D.K., Catani, M., Pierpaoli, C., Reeves, S.J., Shergill, S.S., O'Sullivan, M., Golesworthy, P., McGuire, P., Horsfield, M.A., Simmons, A., et al., 2006. Age effects on diffusion tensor magnetic resonance imaging tractography measures of frontal cortex connections in schizophrenia. Hum. Brain Mapp. 27 (3), 230–238.

Jones, D.K., Knosche, T.R., Turner, R., 2013. White matter integrity, fiber count, and other fallacies: the do's and don'ts of diffusion MRI. NeuroImage 73, 239–254.

Karaus, A., Hofer, S., Frahm, J., 2009. Separation of fiber tracts within the human cingulum bundle using single-shot STEAM DTI. Open Med. Imaging J. 3, 21–27.

Keller, T.A., Just, M.A., 2009. Altering cortical connectivity: remediation-induced changes in the white matter of poor readers. Neuron 64, 624–631.

Kitchen, C.M.R., 2009. Nonparameteric vs parameteric tests of location in biomedical research. Am J. Ophthalmol. 147 (2), 571–572.

Klein, S., Staring, M., Murphy, K., Viergever, M.A., Pluim, J., 2010. Elastix: a toolbox for intensity-based medical image registration. IEEE Trans. Med. Imaging 29, 196–205.

Koch, M., Glauche, V., Finsterbusch, J., Nolte, U., Frahm, J., Buchel, C., 2001. Estimation of anatomical connectivity from diffusion tensor data. NeuroImage 13, S176.

Kristo, G., Leemans, A., de Gelder, B., Raemaekers, M., Rutten, G.J., Ramsey, N., 2013a. Reliability of the corticospinal tract and arcuate fasciculus reconstructed with DTI-based tractography: implications for clinical practice. Eur. Radiol. 23 (1), 28–36.

Kristo, G., Leemans, A., Raemaekers, M., Rutten, G.J., de Gelder, B., Ramsey, N., 2013b. Reliability of two clinically relevant fiber pathways reconstructed with constrained spherical deconvolution. Magn. Reson. Med. http://dx.doi.org/10.1002/mrm.24602 (in press).

Kumar, R., Husain, M., Gupta, R.K., Hasan, K.M., Haris, M., Agarwal, A.K., Pandey, C.M., Narayana, P.A., 2009. Serial changes in the white matter diffusion tensor imaging metrics in moderate traumatic brain injury and correlation with neuro-cognitive function. J. Neurotrauma 26 (4), 481–495.

Lebel, C., Beaulieu, C., 2011. Longitudinal development of human brain wiring continues from childhood into adulthood. J. Neurosci. 31 (30), 10937–10947.

Lebel, C., Walker, L., Leemans, A., Phillips, L., Beaulieu, C., 2008. Microstructural maturation of the human brain from childhood to adulthood. NeuroImage 40 (3), 1044–1055.

Lebel, C., Caverhill-Godkewitsch, S., Beaulieu, C., 2010. Age-related regional variations of the corpus callosum identified by diffusion tensor tractography. NeuroImage 52 (1), 20–31.

Leemans, A., Jones, D.K., 2009. The B-matrix must be rotated when motion correcting diffusion tensor imaging data. Magn. Reson. Med. 61, 1336–1349.

Leemans, A., Sijbers, J., De Backer, S., Vandervliet, E., Parizel, P., 2006. Multiscale white matter fiber tract coregistration: a new feature-based approach to align diffusion tensor data. Magn. Reson. Med. 55 (6), 1414–1423.

Leemans, A., Jeurissen, B., Sijbers, J., Jones, D.K., 2009. ExploreDTI: a graphical toolbox for processing analyzing, and visualizing diffusion MR data. 17th Annual Meeting of Intl. Soc. Mag. Reson. Med., Hawaii, USA, p. 3537.

Ljungqvist, J., Nilsson, D., Ljungberg, M., Sörbo, A., Esbjörnsson, E., Eriksson-Ritz, N.C., Skoglund, T., 2011. Longitudinal study of the diffusion tensor imaging properties of the corpus callosum in acute and chronic diffuse axonal injury. Brain Inj. 25 (4), 370–378.

Madsen, K.S., Baaré, W.F., Vestergaard, M., Skimminge, A., Ejersbo, L.R., Ramsoy, T.Z., Gerlach, C., Akeson, P., Paulson, O.B., Jernigan, T.L., 2010. Response inhibition is associated with white matter microstructure in children. Neuropsychologia 48 (4), 854–862.

Madsen, K.S., Baaré, W.F., Skimminge, A., Vestergaard, M., Siebner, H.R., Jernigan, T.L., 2011. Brain microstructural correlates of visuospatial choice reaction time in children. NeuroImage 58 (4), 1090–1100.

Malykhin, N., Concha, L., Seres, P., Beaulieu, C., Coupland, N.J., 2008. Diffusion tensor imaging tractography and reliability analysis for limbic and paralimbic white matter tracts. Psychiatry Res. 164 (2), 132–142.

Mori, S., Crain, B.J., Chacko, V.P., Van Zijl, P.C., 1999. Three dimensional tracking of axonal projections in the brain by magnetic resonance imaging. Ann. Neurol. 45, 265–269.

Mori, S., Oishi, K., Jiang, H., Jiang, L., Li, X., Akhter, K., Hua, K., Faria, A.V., Mahmood, A., Woods, R., Toga, A.W., Pike, G.B., Neto, P.R., Evans, A., Zhang, J., Huang, H., Miller, M.I., van Zijl, P., Mazziotta, J., 2008. Stereotaxic white matter atlas based on diffusion tensor imaging in an ICBM template. NeuroImage 40 (2), 570–582.

Nimsky, C., Ganslandt, O., Hastreiter, P., Wang, R., Benner, T., Sorensen, A.G., Fahlbusch, R., 2005. Intraoperative diffusion-tensor MR imaging: shifting of white matter tracts during neurosurgical procedures—initial experience. Radiology 234 (1), 218–225.

Nimsky, C., Ganslandt, O., Merhof, D., Sorensen, A.G., Fahlbusch, R., 2006. Intraoperative visualization of the pyramidal tract by diffusion-tensor-imaging-based fiber tracking. NeuroImage 30 (4), 1219–1229.

O'Donnell, L.J., Westin, C.F., Golby, A.J., 2009. Tract-based morphometry for white matter group analysis. NeuroImage 45 (3), 832–844.

Parker, G.J.M., Stephan, K.E., Barker, G.J., Rowe, J.B., MacManus, D.G., Wheeler-Kingshott, C.A.M., Ciccarelli, O., Passingham, R.E., Spinks, R.L., Lemon, R.N., Turner, R., 2002. Initial demonstration of in vivo tracing of axonal projections in the macaque brain and comparison with the human brain using diffusion tensor imaging and fast marching tractography. NeuroImage 15, 797–809.

Parker, G.J., Haroon, H.A., Wheeler-Kingshott, C.A., 2003. A framework for a streamline-based probabilistic index of connectivity (PICO) using a structural interpretation of MRI diffusion measurements. J. Magn. Reson. Imaging 18, 242–254.

Pfefferbaum, A., Adalsteinsson, E., Sullivan, E.V., 2003. Replicability of diffusion tensor imaging measurements of fractional anisotropy and trace in brain. J. Magn. Reson. Imaging 18, 427–433.

Pierpaoli, C., Basser, P.J., 1996. Toward a quantitative assessment of diffusion anisotropy. Magn. Reson. Med. 36 (6), 893–906.

Poupon, C., Clark, C.A., Frouin, V., Regis, J., Bloch, I., Le Bihan, D., Mangin, J., 2000. Regularization of diffusion-based direction maps for the tracking of brain white matter fasciculi. NeuroImage 12, 184–195.

Price, G., Cercignani, M., Parker, G.J., Altmann, D.R., Barnes, T.R., Barker, G.J., Joyce, E.M., Ron, M.A., 2008. White matter tracts in first-episode psychosis: a DTI tractography study of the uncinate fasciculus. NeuroImage 39 (3), 949–955.

Reese, T.G., Heid, O., Weisskoff, R.M., Wedeen, V.J., 2003. Reduction of eddy-current-induced distortion in diffusion MRI using a twice-refocused spin echo. Magn. Reson. Med. 49 (1), 177–182.

Reich, D.S., Ozturk, A., Calabresi, P.A., Mori, S., 2010. Automated vs. conventional tracto-graphy in multiple sclerosis: variability and correlation with disability. NeuroImage 49 (4), 3047–3056.

Reijmer, Y.D., Leemans, A., Cayenberghs, K., Heringa, S.M., Koek, H.L., Biessels, G.J., 2013. Disruption of cerebral networks and cognitive impairment in Alzheimer's disease. Neurology 80 (15), 1370–1377.

Rohde, G.K., Barnett, A.S., Basser, P.J., Marenco, S., Pierpaoli, C., 2004. Comprehensive approach for correction of motion and distortion in diffusion-weighted MRI. Magn. Reson. Med. 51, 103–114.

Sage, C.A., Van Hecke, W., Peeters, R., Sijbers, J., Robberecht, W., Parizel, P.M., Marchal, G., Leemans, A., Sunaert, S., 2009. Quantitative diffusion tensor imaging in amyotrophic lateral sclerosis: revisited. Hum. Brain Mapp. 30 (11), 3657–3675.

Schlaug, G., Marchina, S., Norton, A., 2009. Evidence for plasticity in white-matter tracts of patients with chronic Broca's aphasia undergoing intense intonation-based speech therapy. Ann. N. Y. Acad. Sci. 1169, 385–394.

Scholz, J., Klein, M.C., Behrens, T.E., Johansen-Berg, H., 2009. Training induces changes in white-matter architecture. Nat. Neurosci. 12 (11), 1370–1371.

Smith, S.M., Jenkinson, M., Johansen-Berg, H., Rueckert, D., Nichols, T.E., Mackay, C.E., Watkins, K.E., Ciccarelli, O., Cader, M.Z., Matthews, P.M., Behrens, T.E., 2006. Tract-based spatial statistics: voxelwise analysis of multi-subject diffusion data. NeuroImage 31 (4), 1487–1505.

Snook, L., Paulson, L.A., Roy, D., Phillips, L., Beaulieu, C., 2005. Diffusion tensor imaging of neurodevelopment in children and young adults. NeuroImage 26 (4), 1164–1173.

Suarez, R.O., Commowick, O., Prabhu, S.P., Warfield, S.K., 2012. Automated delineation of white matter fiber tracts with a multiple region-of-interest approach. NeuroImage 59 (4), 3690–3700.

Sullivan, E.V., Pfefferbaum, A., 2007. Neuroradiological characterization of normal adult ageing. Br. J. Radiol. 80, S99–S108.

Sullivan, E.V., Rohling, T., Pfefferbaum, A., 2010. Longitudinal study of callosal micro-structure in the normal adult aging brain using quantitative DTI fiber tracking. Dev. Neuropsychol. 35 (3), 233–256.

Tournier, J.D., Mori, S., Leemans, A., 2011. Diffusion tensor imaging and beyond. Magn. Reson. Med. 65 (6), 1532–1556.

Van der Aa, N.E., Leemans, A., Northington, F.J., van Straaten, H.L., van Haastert, I.C., Groenendaal, F., Benders, M.J., de Vries, L.S., 2011. Does diffusion tensor imaging-based tractography at 3 months of age contribute to the prediction of motor outcome after perinatal arterial ischemic stroke? Stroke 42 (12), 3410–3414.

Van Hecke, W., Leemans, A., D'Agostino, E., De Backer, S., Vandervliet, E., Parizel, P.M., Sijbers, J., 2007. Nonrigid coregistration of diffusion tensor images using a viscous fluid model and mutual information. IEEE Trans. Med. Imaging 26 (11), 1598–1612.

Van Hecke, W., Leemans, A., Sijbers, J., Vandervliet, E., Van Goethem, J., Parizel, P.M., 2008a. A tracking-based diffusion tensor imaging segmentation method for the detection of diffusion-related changes of the cervical spinal cord with aging. J. Magn. Reson. Imaging 27 (5), 978–991.

Van Hecke, W., Sijbers, J., D'Agostino, E., Maes, F., De Backer, S., Vandervliet, E., Parizel, P.M., Leemans, A., 2008b. On the construction of an inter-subject diffusion tensor magnetic resonance atlas of the healthy human brain. NeuroImage 43 (1), 69–80.

Van Hecke, W., Sijbers, J., De Backer, S., Poot, D., Parizel, P.M., Leemans, A., 2009. On the construction of a ground truth framework for evaluating voxel-based diffusion tensor MRI analysis methods. NeuroImage 46 (3), 692–707.

Van Hecke, W., Leemans, A., De Backer, S., Jeurissen, B., Parizel, P.M., Sijbers, J., 2010a. Comparing isotropic and anisotropic smoothing for voxel-based DTI analyses: a simulation study. Hum. Brain Mapp. 31 (1), 98–114.

Van Hecke, W., Nagels, G., Leemans, A., Sijbers, J., Parizel, P.M., 2010b. Correlation of cognitive dysfunction and diffusion tensor MRI measures in patients with mild and moderate multiple sclerosis. J. Magn. Reson. Imaging 31 (6), 1492–1498.

Van Hecke, W., Leemans, A., Sage, C.A., Veraart, J., Sijbers, J., Sunaert, S., Parizel, P.M., 2011. The effect of template selection on diffusion tensor voxel based analysis results. NeuroImage 55 (2), 566–573.

Verhoeven, S., Sage, C.A., Leemans, A., Van Hecke, W., Callaert, D., Peeters, R., De Cock, P., Lagae, L., Sunaert, S., 2010. Construction of a stereotaxic DTI atlas with full diffusion tensor information for studying white matter maturation from childhood to adolescence using tractography-based segmentations. Hum. Brain Mapp. 31 (3), 470–486.

Vos, S.B., Jones, D.K., Viergever, M.A., Leemans, A., 2011. Partial volume effects as a hidden covariate in DTI analyses. NeuroImage 55 (4), 1566–1576.

Wakana, S., Jiang, H., Nagae-Poetscher, L.M., van Zijl, P.C., Mori, S., 2004. Fiber tract-based atlas of human white matter anatomy. Radiology 230 (1), 77–87.

Wakana, S., Caprihan, A., Panzenboeck, M.M., Fallon, J.H., Perry, M., Gollub, R.L., Hua, K., Zhang, J., Jiang, H., Dubey, P., Blitz, A., van Zijl, P., Mori, S., 2007. Reproducibility of quantitative tractography methods applied to cerebral white matter. NeuroImage 36, 630–644.

Wedeen, V.J., Wang, R.P., Schmahmann, J.D., Benner, T., Tseng, W.Y.I., Dai, G., Pandya, D.N., Hagmann, P., D'Arceuil, H., de Crespigny, A.J., 2008. Diffusion spectrum magnetic resonance imaging (DSI) tractography of crossing fibers. NeuroImage 41, 1267–1277.

Yendiki, A., Panneck, P., Srinivasan, P., Stevens, A., Zollei, L., Augustinack, J., Wang, R., Salat, D., Ehrlich, S., Behrens, T., Jbabdi, S., Gollub, R., Fischl, B., 2011. Automated proba-bilistic reconstruction of white-matter pathways in health and disease using an atlas of the underlying anatomy. Front. Neuroinformatics 5–23.

Yogarajah, M., Powell, H.W., Parker, G.J., Alexander, D.C., Thompson, P.J., Symms, M.R., Boulby, P., Wheeler-Kingshott, C.A., Barker, G.J., Koepp, M.J., Duncan, J.S., 2008. Tractography of the parahippocampal gyrus and material specific memory im-pairment in unilateral temporal lobe epilepsy. NeuroImage 40 (4), 1755–1764.

Yogarajah, M., Focke, N.K., Bonelli, S.B., Thompson, P., Vollmar, C., McEvoy, A.W., Alexander, D.C., Symms, M.R., Koepp, M.J., Duncan, J.S., 2010. The structural plasticity of white matter networks following anterior temporal lobe resection. Brain 133, 2348–2364.

Zhang, J., Evans, A., Hermoye, L., Lee, S.K., Wakana, S., Zhang, W., Donohue, P., Miller, M.I., Huang, H., Wang, X., van Zijl, P.C., Mori, S., 2007. Evidence of slow maturation of the superior longitudinal fasciculus in early childhood by diffusion tensor imaging. NeuroImage 38 (2), 239–247.

Zhang, Y., Zhang, J., Oishi, K., Faria, A.V., Jiang, H., Li, X., Akhter, K., Rosa-Neto, P., Pike, G.B., Evans, A., Toga, A.W., Woods, R., Mazziotta, J.C., Miller, M.I., van Zijl, P.C., Mori, S., 2010. Atlas-guided tract reconstruction for automated and comprehensive exami-nation of the white matter anatomy. NeuroImage 52 (4), 1289–1301.